HANDHELD GAMMA-RAY SPECTROMETRY FOR ASSAYING RADIOACTIVE MATERIALS IN LUNGS

A Thesis
Presented to
The Academic Faculty

by

Jesson D. Hutchinson

In Partial Fulfillment
of the Requirements for the Degree
Master of Science in the
George W. Woodruff School of Mechanical Engineering

Georgia Institute of Technology
December 2005

HANDHELD GAMMA-RAY SPECTROMETRY FOR ASSAYING RADIOACTIVE MATERIALS IN LUNGS

Approved by:

Dr. Nolan E. Hertel, Advisor
Nuclear and Radiological Engineering
Georgia Institute of Technology

Dr. C.-K. Chris Wang
Nuclear and Radiological Engineering
Georgia Institute of Technology

Dr. Armin J. Ansari
Centers for Disease Control and Prevention

Date Approved: November 10, 2005

ACKNOWLEDGEMENTS

First I must thank God for guiding me throughout these years in all of the decisions that I've made. Next I want to thank my parents and my sister for all of their support since the day I was born. You guys have taught me much more than you will ever know and I will always be grateful.

I would like to thank my advisor, Dr. Nolan Hertel, for all of his help and guidance over the last few years. I am proud to be a member of Team Hertel. I would also like to thank the members on my thesis committee, Dr. Chris Wang and Dr. Armin Ansari for their interest in my work. I am also very grateful to Zhonglu Wang, my unofficial second advisor. Zhonglu helped me so much on this project and never got annoyed when I asked for his help (which happened often). I would also like to thank all of the students that helped me along the way, especially Ryan Lorio and Eric Burgett. Thanks are also due to Dr. Rebecca Howell for getting a CT scan of our phantom. Last, I'd like to thank my family and friends for just being themselves. You guys are the reason that my life is awesome.

TABLE OF CONTENTS

LIST OF TABLES

LIST OF FIGURES

SUMMARY

After a Radiological Dispersal Device (RDD) event, there will not be time to transport people to a whole-body-counter (WBC), since it is a specialized instrument. This work will assess the feasibility of using handheld spectrometers for measuring the radioactivity that may have been inhaled by a victim as a consequence of an RDD event. Measurements were made with a handheld isotope identifier using a slab phantom and several radioactive point sources. A Lawrence Livermore National Laboratory (LLNL) Realistic Torso Phantom and a set of phantoms based on Medical Internal Radiation Dose (MIRD) reports were also used in this work. These phantoms include the human skeleton and have tissue-equivalent organs. Computational models were developed of all of the phantoms using the Monte Carlo Transport code MCNP. After validation of the computer model, MCNP runs were conducted using other sources that are likely to be used in a RDD. Calculations were then done to find the Minimum Detectable Activity (MDA) of all sources used. The Minimum Detectable Dose (MDD) was then calculated for the MIRD phantoms at various times after inhalation.

CHAPTER 1

INTRODUCTION

A Radiological Dispersal Device (RDD) is any device that would potentially release radionuclides into the environment and is the most likely means of terrorist attack involving nuclear or radiological weapons. Between October 1996 and September 2001, 1,495 radioactive sources were reported lost or stolen in the U.S., any of which could be used for a dispersal device (Brodsky et al., 2004). This work assesses the ability of using a handheld detector for measuring radioactive materials inhaled from an RDD event. The detector used is a gamma detector, therefore only gamma emitting sources were studied in this work. The photon emitting radioisotopes of highest concern for RDDs include ^{137}Cs, ^{60}Co, ^{241}Am, and ^{192}Ir (Ferguson, 2003). Also of concern is ^{90}Sr/^{90}Y, which emits electrons through beta decay. These electrons will, however, produce bremsstrahlung photons. All of these radionuclides, in addition to ^{131}I, are considered in this work.

After an RDD event occurs, there will be many people rushing to hospitals and other locations who are unsure if they have inhaled radioactive materials. Hospitals will most likely not be equipped to prescribe medication to all of these people. A method needs to be developed to triage patients to determine which patients should receive medication. If medication is needed, it generally needs to be taken soon after the radioactive materials enter the body.

A Whole Body Counter (WBC) is a device designed for identifying and measuring the concentration of radioactive materials located inside a person's body. It uses very sensitive radiation detectors and has shielding to reduce the background radiation. Even though WBCs would be the best device to measure the radioactivity levels inhaled by a victim of an RDD event, they are usually only available at distant locations from urban centers and the number of people to be counted would make them

an impractical approach to the problem. Handheld detectors are readily available in large cities. Handheld spectrometers are not as sensitive as a WBC, but they could be used to quickly determine the radioactivity levels in lungs of victims. To determine the usefulness of a handheld detector for this specific application, computational models of several phantoms were run. From these data, the Minimum Detectable Activity (MDA) was determined for the handheld detector. The Minimum Detectable Intake (MDI) was back calculated from the MDA for several times after intake over the period of one week. The Minimum Detectable Dose (MDD) was then calculated from the MDI for these counting times.

CHAPTER 2

HANDHELD SPECTROMETER

The detector used in this work was the Exploranium GR-130 miniSPEC. This portable gamma-ray spectrometer is used to locate and identify radionuclides in real-time. This detector has a 4.5 cubic inch sodium-iodide crystal doped with thallium (NaI(Tl)) and weighs 5.5 lbs. It can be used to measure the count rate or perform a spectral analysis of a radiation source. The GR-130 detector and the orientation referenced in this paper are shown in Figure 2.1. The efficiency is highest at the front of the detector, so the front face should be placed against or directed toward the radiation source being measured.

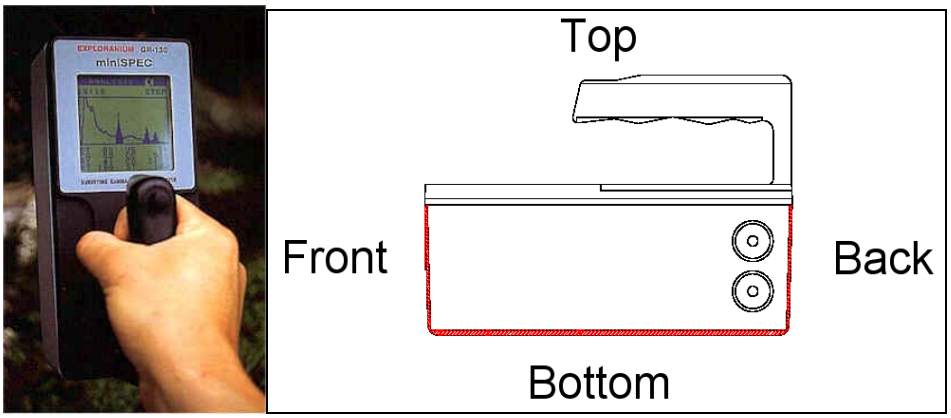

Figure 2.1: Detector Orientation

Popular uses for this device include surveying contaminated soil and hazard identification in addition to spectral analysis. It can operate in survey mode, dose rate mode, and nuclide identification mode. Before any measurements are made, the detector

must be calibrated using a 0.214 μCi ^{137}Cs source, which accompanies the instrument from the manufacturer. The sensitivity of the GR-130 to high-energy gamma rays is low, as with many sodium iodide detectors (Peterson et al., 2005).

While this detector could work well for triaging patients after an RDD event, it also has several disadvantages for this application. In the spectrum mode, if a pulse-height exceeds 65,535 counts in any channel (or if 65,535 cps are recorded in survey mode), saturation occurs and a display message will appear. The system will also overload if the dead time exceeds seventy percent. These factors place a limit on the activity and counting time that can be measured. Also, the air at a measurement location after an RDD event could have a radiation background in excess of the natural background. This would require subtraction of background counts at the measurement location. Similarly, if the patient has any external contamination it will read a higher activity than that which is present in the lungs. This could be corrected if a person is measured for external contamination before lung counting is performed.

CHAPTER 3

EXPERIMENTAL SETUP

A slab phantom and several anthropomorphic phantoms were used to simulate the transport of photons inside the human body for this work. The slab phantom was measured at various slab thicknesses using point sources to validate the computational model. Several distributed sources inside the anthropomorphic phantoms were then studied.

Slab Phantom

The slab phantom is composed of thin slabs of Plexiglas that can be configured to provide different attenuation thicknesses between the source and detector. Each slab has a height and width of 30 cm with thicknesses ranging from 3 mm to 2.5 cm. When all of the slabs are loaded they have a combined thickness of 13.8 cm, and when the thickness of the outer two Plexiglas casings are included the total thickness is 15 cm. The actual material of the slab phantom is polymethyl-methacrylate (PMMA), $(C_5O_2H_8)_n$, and was assumed to have a nominal density of 1.19 g/cm³.

Measurements were made using both a ^{60}Co and a ^{137}Cs point source taped on the center of the outer Plexiglas casing. The activities of the ^{60}Co and ^{137}Cs sources were 8.914 μCi and 10.15 μCi respectively. Both sources had assay dates of May 1st 2001 but the uncertainties of the source activities were not reported. The detector was placed on the other side of the case, in which the center of the detector crystal was lined up with the source (Figure 3.1). A one-minute reading was done when no slabs were in the case and when the case was fully loaded (13.8 cm). In addition, measurements were taken when

there were 2.5, 5, 7.5, and 10 cm thick slabs inside the case. These distances include only the thickness of the slabs loaded inside the case. The true Plexiglas thickness between the source and the detector would be the slab thickness plus 1.2 cm (for the 6 mm thick Plexiglas casing on both sides).

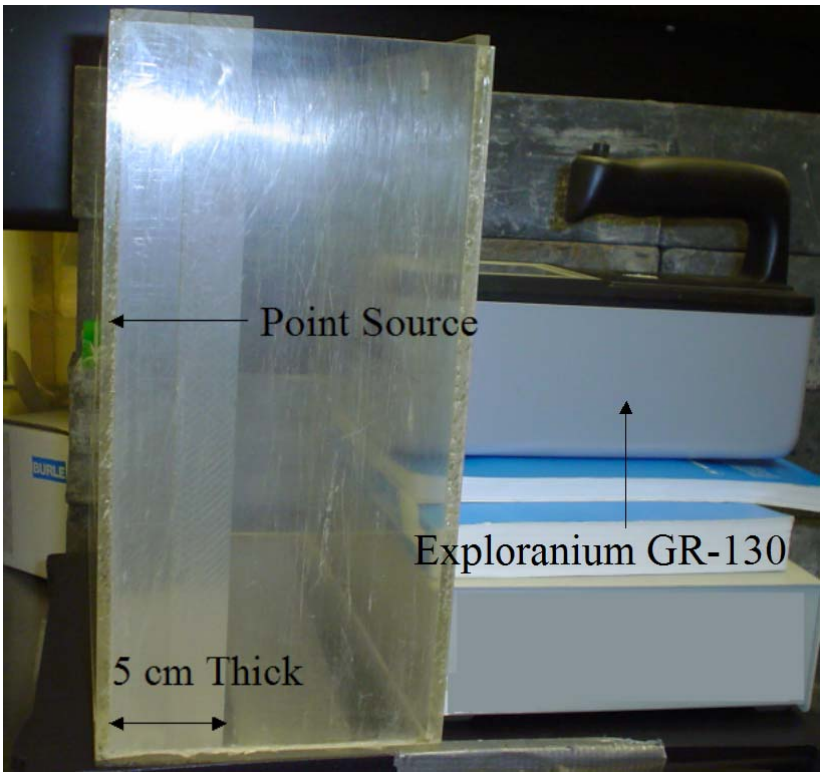

Figure 3.1: Slab Experiment Configuration

Background measurements were taken immediately before and after the slab measurements were made. These background measurements were used for all of the work presented here. The measurements were taken at a laboratory at Georgia Institute of Technology. The background spectrum in this lab could differ greatly from that at the location in which actual patients would be measured. Differences in background values

could have a large influence on all of the results obtained. This is discussed in greater detail in Chapter 5.

Realistic Torso Phantom

The LLNL Realistic Torso Phantom is an anthropomorphic phantom that is used to calibrate detectors for the measurement of radionuclides which are deposited in organs and is considered to be "the *de facto* standard phantom for lung counting" (Kramer et al., 1991). Anthropomorphic phantoms are designed to represent the radiation attenuation and geometry of the human body. This phantom is based on a deceased LLNL plutonium worker and as a result is larger than reference man listed in ICRP 23 and later updated in ICRP 89 (Kramer et al., 1997; ICRP, 1975; ICRP, 2003). This phantom includes the human head and torso and is molded around a synthetic skeleton. The interior of the phantom is hollow and filled with both simulated organs and spacer blocks, which are equivalent to human tissue. The heart, kidneys, and thyroid organs are hollow and can be filled with water. Radioactive sources can be placed inside the liver and lungs of the phantom. The tissue, skeleton, lungs, and liver are all made of polyurethane-based substitutes (ICRU, 1992). The chest plate cover has a thickness of 1.63 cm (Kramer et al., 1998). Figure 3.1 shows the Realistic Torso Phantom that was used to construct a computational model for this work.

Figure 3.2: The LLNL Realistic Torso Phantom

While the Realistic Torso Phantom is one of the most popular phantoms for lung counting it does have several deficiencies. The lungs of the phantom are short compared to those of most people. They are approximately 10 cm shorter than the lungs in ICRP 23 (Kramer, 2004; ICRP, 1975). The phantom was modeled on a cadaver that was similar to the average plutonium worker at LLNL. Even though the cadaver was kept cool, some decomposition occurred between the time of death and the modeling. This decomposition led to a "gas build up that pushed the heart and lungs higher in the chest cavity, hence leading to short lungs" (Kramer, 2004). This decomposition is also the reason for the large chest curvature of the phantom. The phantom also has a large heart that blocks out a significant fraction of the left lung. The left and right lungs have a volume ratio of 43.5 to 56.5 (Kramer et al., 1998). The chest wall thickness is almost constant around the whole phantom, unlike real people which are usually thinner in the middle and thicken towards the outer edges (Kramer et al., 1998).

There are very little data on NaI(Tl) detectors being used in conjunction with the LLNL Realistic Torso Phantom. When the phantom was first manufactured lung

counting was commonly performed using phoswich detectors. That is why the chest plate contains circles that show the optimum placement for this type of detector. Technology has improved since the phantom development and now germanium detector arrays are much more common for lung counting. No literature could be found in which a small sodium-iodide detector was used with the LLNL phantom.

CHAPTER 4

COMPUTATIONAL MODELS

The computational modeling was performed with the Monte Carlo N-Particle transport code version 5 (MCNP5) (X-5 Monte Carlo Team, 2003). When creating an input file, the user specifies the geometry and material makeup/density of the system. The user also gives details on the radiation source and tally, which is how you specify what results you want. An f8 tally, known as a pulse-height tally, was used in all models. This tally records the energy deposited in a cell by each source particle and its secondary particles (X-5 Monte Carlo Team, 2003). Table 4.1 shows information on the primary gammas emitted for the radioisotopes used in the MCNP models. The Region of Interest (ROI) is the energy range that is integrated over in determining the detector efficiency.

Table 4.1: Radioisotope Gamma Data

	Cs-137	Co-60	Am-241	Ir-192	I-131
γ-ray Energy (keV)	662	1173, 1333	59.5	296-612	364.5, 637
γ-ray Intensity	0.851	1, 1	0.359	2.13	0.812, 0.073
ROI (keV)	601-723	1075-1427	36-73	267-650	322-407

A Gaussian Energy Broadening (GEB) treatment was used to simulate the resolution of the detector. This treatment uses three parameters to define the resolution of the detector at a specific energy by:

$$fwhm = a + b\sqrt{E + cE^2} \qquad [4.1]$$

where:

E = the peak energy (MeV)

$fwhm$ = the full width at half maximum of a Gaussian resolution function centered at E

a = unknown parameter

b = unknown parameter

c = unknown parameter

To solve for a, b, and c, measured spectra for ^{137}Cs and ^{60}Co point sources were used to determine the fwhm of the three photopeaks (662 keV peak for ^{137}Cs, 1.17 MeV and 1.33 MeV peaks for ^{60}Co). The parameters were then solved using GNUfit and were found to be a = -0.0050254, b = 0.0700037, and c = -0.0784113. Plugging these values in at an energy of 662 keV gives a resolution of 7.59%. The GR-130 manual states that the resolution at 662 keV should be 7.2%±0.5% (Exploranium Radiation Detection Systems, 2001).

Handheld Detector

The model of the Exploranium GR-130 was constructed as best as possible without having detailed blueprints of the detector available. The manual of the detector reported that the crystal had a diameter and height of 3.8 cm (1.5 inch) and 5.7 cm (2.2 inch), respectively. The detector is placed 0.21 cm from the front face of the detector box and was centered in the other two directions. Data were taken using a ^{137}Cs point source located 20 cm and 10 cm from the front face of the detector case. This same

configuration was then modeled in MCNP. Integrating over the ^{137}Cs 662 keV peak gives a difference between measured and calculated data of 2.1% and 0.7% at 20 cm and 10 cm, respectively.

Slab Phantom Model

For the model of the slab phantom, the detector was placed in the same way as described in the experimental setup. In the computational model multiple slabs were considered to be one large parallelepiped, which does not take small air gaps in between the slabs into consideration. Figure 4.1 shows the setup with a combination of slabs totaling 5-cm thick inside the case. After the model was validated against the measured data additional runs were performed with a 15-cm thick slab behind the point source. This showed the contribution of backscattering and allows for a more realistic model, since a person has tissue behind their lungs. Models were run when the case was empty, with slab thicknesses of 0.5, 1, 1.5, 2, 2.5, 3, 4, 5, 7.5, and 10 cm, and with all of the slabs loaded (13.8 cm).

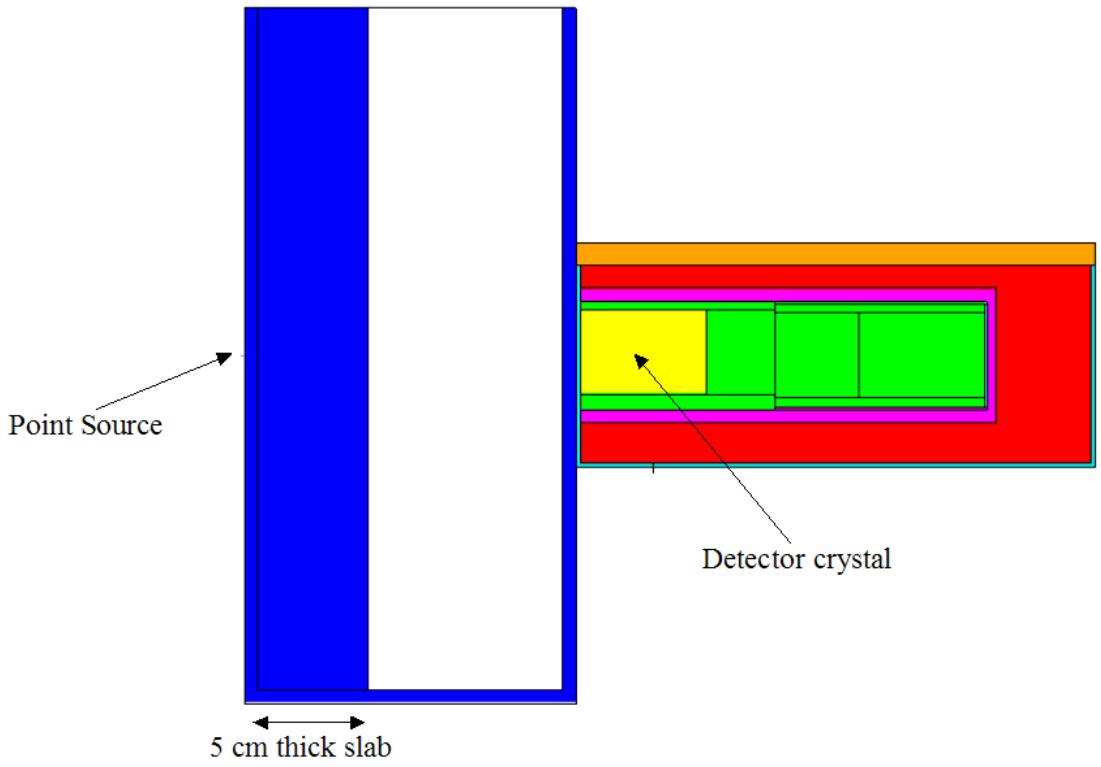

Figure 4.1: MCNP Model with a 5 cm Thick Slab

LLNL Phantom Model

A voxel phantom was used to model the LLNL phantom because it would be too difficult to model using regular geometry. To achieve this, a CT scan was taken of the phantom at Emory University Hospital. The Digital Imaging and Communications in Medicine (DICOM) files from the scan were then loaded into the Scan2MCNP program, developed by White Rock Science (White Rock Science, 2003).

Scan2MCNP converts the CT scan data contained in the DICOM images into an MCNP input file. Each DICOM file is a two dimensional image or slice taken during the CT scan. The operator can set the spacing of the slices; for our scan, a slice was taken every 5 mm. For this work the x, y, and, z axes are the transverse, anteroposterior, and vertical axes respectively. Each pixel of a DICOM image has a corresponding intensity that is related to the density of the material. The user can create partitions that represent ranges of pixel intensities. Then each partition can be used to represent a specific material. The input file generated contains only the geometry and materials of the region that was scanned. Figure 4.2 shows a DICOM image, the image loaded in the Scan2MCNP program, the image with partitions, and the same slice as an MCNP input file.

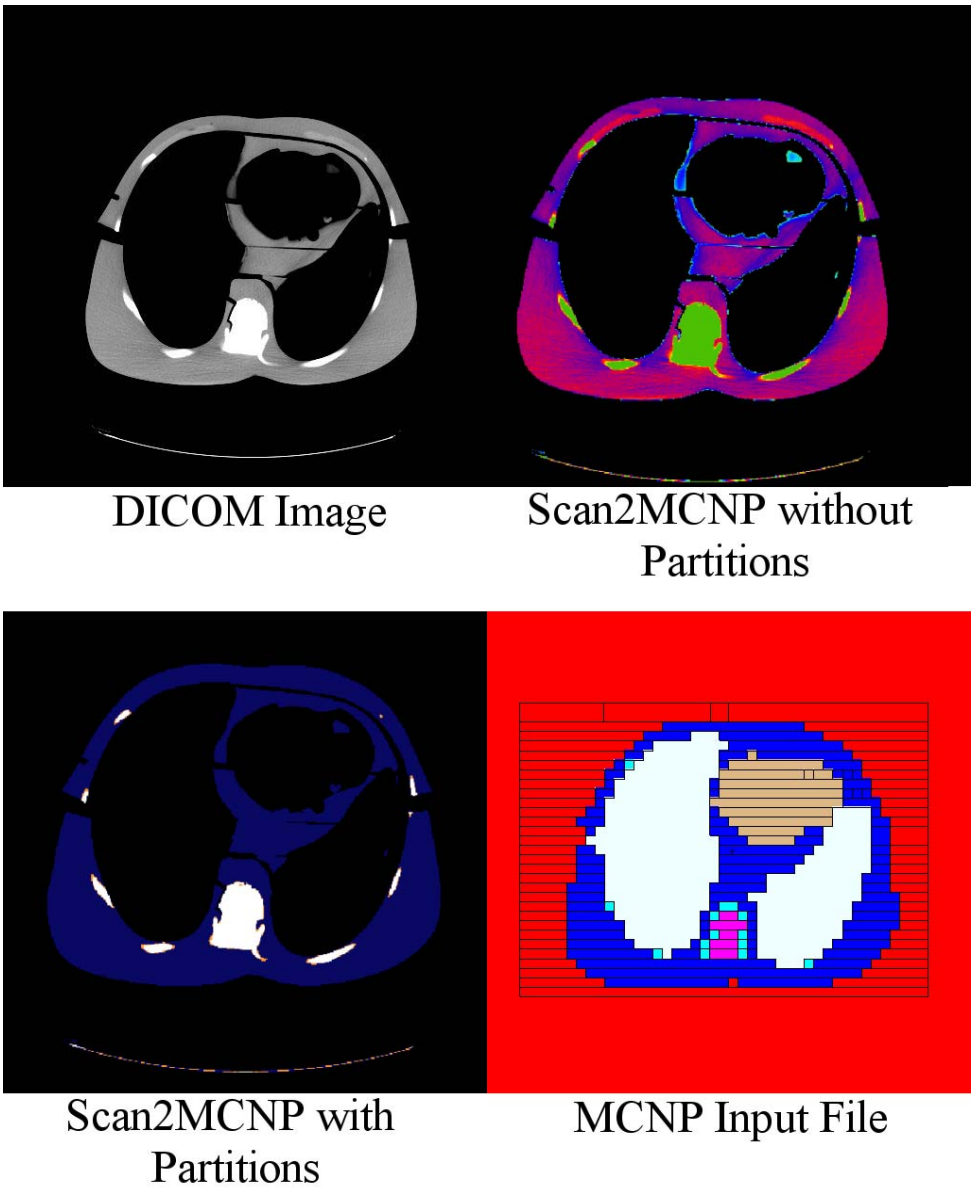

Figure 4.2: A Slice of the LLNL Phantom from a DICOM Image to an MCNP Input

The user specifies how big to make the voxels; for this work voxels are 1 cm in the x and y directions and 2 cm in the z direction. These dimensions were chosen to keep the number of cells in the input file low. If the input file had more than around 5,000 cells, problems were experienced and the code would not run properly. If a voxel contains more than one material, the user can choose to either create a new fraction-weighted material or use the material that has the highest fraction. The program also contains an algorithm that can be used to combine neighboring cells of the same material. The use of this algorithm helps reduce the number of cells in the MCNP input file. This was only used for combining cells in the x and y directions, since combining cells in the z direction is not very efficient. The Scan2MCNP manual states that "combining in the z results in only a few more cells being combined at the expense of a much larger computational time" (White Rock Science, 2003).

When the scan was taken, all of the organs were empty, which is why the heart shows up as air in the picture above. The kidneys and heart were filled with water manually in the MCNP input. The density of the lung material was so low that it also appeared as air and was converted to lung equivalent tissue. Other manual touchups were done to the input including areas where air gaps were present. Table 4.2 shows the densities of the various materials used in the model of the phantom.

Table 4.2: Densities of Materials in LLNL Model

	Density (g/cm^3)
Tissue	1.04
Skeleton	1.40
Lungs	0.25
Liver	1.11
Kidneys	1.00
Heart	1.00

The model used extends from the waistline to the neck of the phantom. This was done to reduce the number of total cells in the model. Large parallelepipeds using the same tissue material were added above and below this region to represent the head and waist of the phantom. All of the cells that comprise the lungs were combined into 10 large cells. The source definition used contains the V option, which makes probabilities proportional to the cell volume, so that a distributed source in the lungs is achieved. This assumption that the radioactive material deposition is uniformly distributed in the lungs may not be valid. The particle distribution is a function of particle size, breathing rate, and health of the person (Kramer et al., 1997). The results obtained from a uniformly contaminated lung versus a lung with highly localized activity could be drastically different. It was reported that when assuming a homogenous distribution in the lungs the activity can be underestimated by a factor of four or overestimated by a factor of 26 when radioisotopes are actually heterogeneously located (Kramer et al., 1997).

The model of the detector was then inserted into the model of the LLNL phantom. The front face of the detector was placed against the chest of the phantom. This configuration might not seem optimal, since it is more natural to hold the detector in such a way that the bottom of the detector touches the chest. It is also more difficult to read the display when the front of the detector is against the chest. The efficiency obtained from this method is, however, significantly higher due to the detector location. The center of the detector was lined up on the chest surface with the center of the right lung. This gives a better efficiency than over the left lung because of the lung volume ratio described in Chapter 3. It was reported that centering the detector above the midpoint of the right lung gave maximum efficiency regardless of photon energy when using

germanium detectors (Kramer et al., 1999). It was assumed that the same was true when using a sodium-iodide detector.

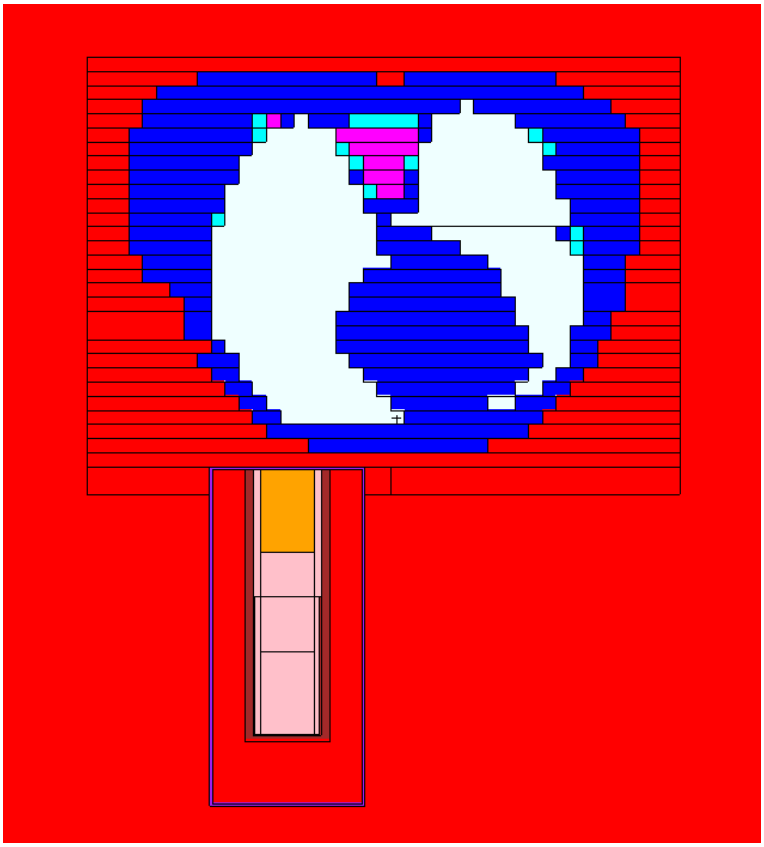

Figure 4.3: MCNP Model of the LLNL Phantom with the GR-130 Detector

MIRD Phantom Models

Models of anthropomorphic phantoms based on the Medical Internal Radiation Dose (MIRD) reports were also constructed. Five different models were made using the BodyBuilder program (White Rock Science, 2004). Models of a male, female, adipose male, adipose female, and 10-year-old androgynous child were used for this work. All of the organs available in the BodyBuilder program were included in the models. Unlike the LLNL model, the MIRD models are not composed of voxels. The detector was lined up with the center of the right lung similar to the LLNL phantom. For the two female models the detector was placed against the back for higher efficiency. A picture of the model and detector placement used on the male MIRD phantom is shown below (Figure 4.4).

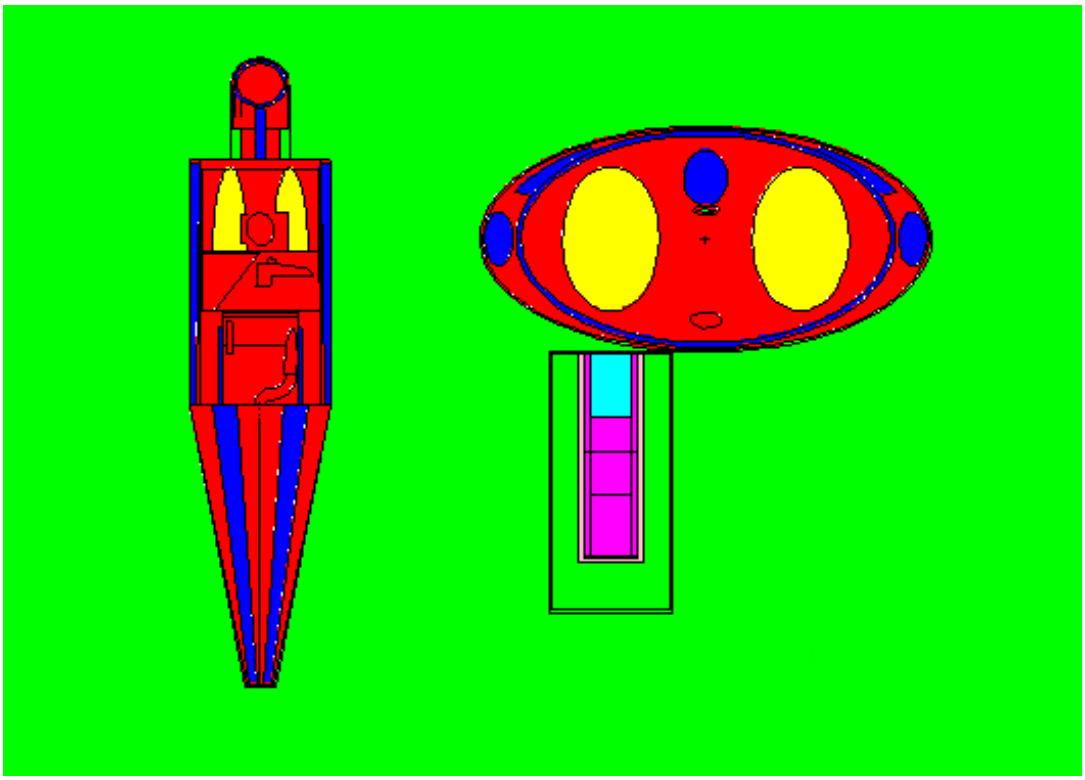

Figure 4.4: Male MIRD Phantom

CHAPTER 5

RESULTS

The data obtained from the GR-130 can be sent to a computer using the SpecView program. The spectral analysis given from this program is given in counts per minute. The data are given in 256 channels, but the energy of each channel is not specified. Known peaks were used to assign the energy of each channel.

The energy bins in the MCNP input file were assigned to match the channels of the detector. The data from the MCNP tally are given in pulse-height per source gamma-ray or beta particle. This can be converted to counts per minute by multiplying by the activity (in decays per minute) and the emission probability.

Slab Results

The MCNP model was compared to measured data for two point sources at six different slab thicknesses. Table 5.1 shows the ratio of measured efficiency to computed efficiency for ^{137}Cs and ^{60}Co found by integrating over the ROIs shown in Table 4.1. The uncertainty in the listed activity for both point sources was unknown. A nominal uncertainty of 3% was assumed for both sources.

Table 5.1: Measured/Computed Efficiency

Slab Thickness (cm)	0	2.5	5	7.5	10	13.8
Cs-137	1.00±0.033	0.99±0.033	1.02±0.034	1.06±0.035	1.04±0.036	1.05±0.038
Co-60	0.97±0.034	0.95±0.035	0.95±0.036	0.98±0.037	0.97±0.038	0.99±0.040

From Table 5.1 it can be seen that the measured and computed values always had a difference of 6% or less. The average difference between the measured and computed efficiencies was 3.2%. The measured values were generally higher than the computed values for ^{137}Cs while the opposite was true for ^{60}Co, which could partially be due to the error associated with the reported activities. After this code validation, a more complex model was constructed in which a 15 cm thick slab was placed behind the point source. This model was run with the following sources: ^{137}Cs, ^{60}Co, ^{241}Am, ^{192}Ir, and ^{131}I.

The efficiency was calculated for a variety of thicknesses (Table 5.2). The efficiency of all the primary gamma emitters decreases as slab thickness increases. This is expected since more photons will be absorbed for larger slab thicknesses. The calculated error only includes the statistical uncertainty, which is governed by the efficiency and number of particles run. Other factors such as the error in the cross-section libraries were not accounted for.

Table 5.2: Calculated Efficiency of the Slab Model

Slab Thickness	Absolute Efficiency (%)				
(cm)	Cs-137	Co-60	Am-241	Ir-192	I-131
0.0	0.091 ± 1E-03	0.054 ± 7E-04	0.658 ± 3E-03	0.206 ± 1E-03	0.169 ± 1E-03
0.5	0.088 ± 9E-04	0.053 ± 7E-04	0.655 ± 3E-03	0.201 ± 1E-03	0.163 ± 1E-03
1.0	0.085 ± 9E-04	0.052 ± 7E-04	0.645 ± 3E-03	0.195 ± 1E-03	0.156 ± 1E-03
1.5	0.082 ± 9E-04	0.050 ± 7E-04	0.631 ± 3E-03	0.188 ± 1E-03	0.149 ± 1E-03
2.0	0.078 ± 9E-04	0.048 ± 7E-04	0.609 ± 2E-03	0.182 ± 1E-03	0.142 ± 1E-03
2.5	0.075 ± 9E-04	0.047 ± 7E-04	0.591 ± 2E-03	0.175 ± 1E-03	0.135 ± 1E-03
3.0	0.072 ± 8E-04	0.045 ± 7E-04	0.568 ± 2E-03	0.168 ± 1E-03	0.130 ± 1E-03
4.0	0.066 ± 8E-04	0.043 ± 7E-04	0.522 ± 2E-03	0.155 ± 1E-03	0.118 ± 1E-03
5.0	0.060 ± 8E-04	0.040 ± 6E-04	0.477 ± 2E-03	0.144 ± 1E-03	0.107 ± 1E-03
7.5	0.048 ± 7E-04	0.034 ± 6E-04	0.371 ± 2E-03	0.119 ± 1E-03	0.085 ± 9E-04
10.0	0.040 ± 6E-04	0.029 ± 5E-04	0.282 ± 2E-03	0.097 ± 1E-03	0.066 ± 8E-04
13.8	0.028 ± 5E-04	0.023 ± 5E-04	0.188 ± 1E-03	0.072 ± 8E-04	0.046 ± 7E-04

LLNL Phantom Results

The MCNP model of the LLNL phantom was run with the same sources used in the slab model (^{137}Cs, ^{60}Co, ^{241}Am, ^{192}Ir, and ^{131}I). The efficiency data of the LLNL phantom are shown below (Table 5.3).

Table 5.3: Efficiency of the LLNL Phantom Model

Absolute Efficiency (%)				
Cs-137	Co-60	Ir-192	Am-241	I-131
0.077 ± 4E-04	0.047 ± 3E-04	0.183 ± 6E-04	0.396 ± 9E-04	0.142 ± 5E-04

MIRD Phantom Results

The results using the five different MIRD models are shown below (Table 5.4). Appendix C contains the spectral data for all of the anthropomorphic phantoms.

Table 5.4: Efficiency of the MIRD Phantom Models

Model	Absolute Efficiency (%)				
	Cs-137	Co-60	Ir-192	Am-241	I-131
Male	0.076 ± 4E-04	0.050 ± 3E-04	0.186 ± 6E-04	0.386 ± 9E-04	0.139 ± 5E-04
Female	0.093 ± 4E-04	0.060 ± 3E-04	0.226 ± 7E-04	0.463 ± 1E-03	0.170 ± 6E-04
Adipose Male	0.029 ± 2E-04	0.021 ± 2E-04	0.072 ± 4E-04	0.127 ± 5E-04	0.049 ± 3E-04
Adipose Female	0.034 ± 3E-04	0.025 ± 2E-04	0.084 ± 4E-04	0.144 ± 5E-04	0.059 ± 3E-04
Child	0.104 ± 5E-04	0.067 ± 4E-04	0.253 ± 7E-04	0.522 ± 1E-03	0.190 ± 6E-04

Phantom Comparison

The efficiencies of the LLNL phantom and the male MIRD phantom lie within 5% of each other for all of the isotopes used. When comparing the efficiencies of the

slab model with that of the anthropomorphic phantoms, it can be seen that the efficiency of the LLNL and male MIRD phantoms with a distributed source generally falls between a slab thickness of 1.5 to 3 cm in the slab phantom using a point source.

Minimum Detectable Activity

The Minimum Detectable Activity (MDA) is the minimum activity that can be distinguished above background 95% of the time. This value is dependent upon the background count rate and the efficiency of the detector in the ROI. The MDA is determined by:

$$MDA = \frac{3 + 4.65\sqrt{Bt_c}}{t_c \varepsilon P_\gamma} \qquad [5.1]$$

where:

B = background counting rate in the ROI (cps)

ε = absolute efficiency (the sum of the f8 tally over the ROI)

t_c = counting time (s)

P_γ = emission probability of the gammas in the ROI

The MDA was calculated for a counting time of 1, 5, and 10 minutes and reported in nCi. These data are shown in Tables 5.5 for the slab phantom and the errors of these values are reported in the appendix (Table A.1). The error includes the statistical error from the MCNP run as well as the background count rate error. The gamma-ray emission probability error was assumed to be negligible. The MDAs for the MIRD phantoms are shown in Table 5.6. The time column in these tables represents the counting time used.

Table 5.5: MDA Calculated From Computational Results in a Slab Phantom

Time (minutes)	Slab Thickness (cm)	MDA (nCi)				
		Cs-137	Co-60	Am-241	Ir-192	I-131
1	0.0	46.9	30.3	28.4	24.2	43.7
	0.5	48.2	30.7	28.6	24.8	45.3
	1.0	50.2	31.7	29.0	25.6	47.3
	1.5	52.2	32.7	29.7	26.5	49.4
	2.0	54.4	33.8	30.7	27.4	51.8
	2.5	56.9	35.0	31.7	28.5	54.4
	3.0	59.4	36.1	33.0	29.6	56.9
	4.0	64.7	38.1	35.9	32.1	62.4
	5.0	70.5	40.6	39.2	34.7	68.8
	7.5	87.9	47.9	50.4	42.0	86.8
	10.0	107.6	55.5	66.4	51.3	111.2
	13.8	149.8	72.3	99.6	69.7	159.7
5	0.0	20.6	13.2	12.6	10.7	19.3
	0.5	21.1	13.4	12.6	11.0	20.0
	1.0	22.0	13.8	12.8	11.4	20.9
	1.5	22.9	14.3	13.1	11.8	21.8
	2.0	23.8	14.8	13.6	12.2	22.9
	2.5	24.9	15.3	14.0	12.7	24.0
	3.0	26.0	15.8	14.6	13.1	25.1
	4.0	28.3	16.7	15.9	14.3	27.6
	5.0	30.9	17.7	17.3	15.4	30.4
	7.5	38.5	20.9	22.3	18.6	38.3
	10.0	47.1	24.2	29.4	22.8	49.1
	13.8	65.6	31.6	44.1	31.0	70.5
10	0.0	14.5	9.3	8.9	7.6	13.6
	0.5	14.8	9.4	8.9	7.8	14.1
	1.0	15.5	9.7	9.0	8.0	14.7
	1.5	16.1	10.1	9.3	8.3	15.4
	2.0	16.8	10.4	9.6	8.6	16.1
	2.5	17.5	10.7	9.9	8.9	16.9
	3.0	18.3	11.1	10.3	9.3	17.7
	4.0	19.9	11.7	11.2	10.1	19.4
	5.0	21.7	12.5	12.2	10.9	21.4
	7.5	27.1	14.7	15.7	13.2	27.0
	10.0	33.2	17.0	20.7	16.1	34.6
	13.8	46.2	22.2	31.1	21.9	49.7

Table 5.6: MDA Calculated Using MIRD Phantom Models

	Time (minutes)	MDA (nCi)				
		Cs-137	Co-60	Ir-192	Am-241	I-131
Male	1	56.2 ± 6.0%	32.9 ± 6.7%	26.8 ± 2.8%	48.4 ± 3.2%	52.8 ± 3.6%
	5	24.6 ± 6.0%	14.4 ± 6.7%	11.9 ± 2.8%	21.4 ± 3.2%	23.3 ± 3.6%
	10	17.3 ± 6.0%	10.1 ± 6.7%	8.4 ± 2.8%	15.1 ± 3.2%	16.4 ± 3.6%
Female	1	45.9 ± 6.0%	27.0 ± 6.7%	22.1 ± 2.8%	40.4 ± 3.2%	43.2 ± 3.6%
	5	20.1 ± 6.0%	11.8 ± 6.7%	9.8 ± 2.8%	17.9 ± 3.2%	19.1 ± 3.6%
	10	14.1 ± 6.0%	8.3 ± 6.7%	6.9 ± 2.8%	12.6 ± 3.2%	13.5 ± 3.6%
Adipose Male	1	147.2 ± 6.1%	77.4 ± 6.8%	68.9 ± 2.8%	146.9 ± 3.2%	148.9 ± 3.6%
	5	64.5 ± 6.1%	33.8 ± 6.8%	30.6 ± 2.8%	65.0 ± 3.2%	65.7 ± 3.6%
	10	45.4 ± 6.1%	23.8 ± 6.8%	21.6 ± 2.8%	45.8 ± 3.2%	46.3 ± 3.6%
Adipose Female	1	126.6 ± 6.1%	65.5 ± 6.8%	59.4 ± 2.8%	129.8 ± 3.2%	125.8 ± 3.6%
	5	55.4 ± 6.1%	28.6 ± 6.8%	26.4 ± 2.8%	57.4 ± 3.2%	55.5 ± 3.6%
	10	39.0 ± 6.1%	20.1 ± 6.8%	18.6 ± 2.8%	40.5 ± 3.2%	39.2 ± 3.6%
Child	1	41.1 ± 6.0%	24.3 ± 6.7%	19.7 ± 2.8%	35.8 ± 3.2%	38.7 ± 3.6%
	5	18.0 ± 6.0%	10.6 ± 6.7%	8.8 ± 2.8%	15.8 ± 3.2%	17.1 ± 3.6%
	10	12.7 ± 6.0%	7.5 ± 6.7%	6.2 ± 2.8%	11.2 ± 3.2%	12.1 ± 3.6%

Minimum Detectable Dose

After determining the minimum detectable activity for all of the isotopes, it is important to determine the minimum detectable dose (MDD). The MDD will be the determining factor in evaluating the usefulness of handheld detectors for this application. As time passes the inhaled materials will be dissolved into the blood while undergoing radioactive decay. For the isotopes considered in this work the biological absorption will be the limiting factor in a time span of one week after inhalation. Particles are classified into three classes based on their solubility into blood from the repertory tract. Type F particles are readily absorbed, type M have intermediary absorption rates, and type S are nearly insoluble. Intake retention fractions (IRF) were corrected for radioactive decay using Equation 5.2, which is determined by intake data developed for ICRP 68 (Potter, 2002). This led to the IRF values shown in Table 5.7.

$$IRF_R = IRF_T e^{-\lambda t} \quad [5.2]$$

where:

IRF_R = intake retention fraction corrected for radioactive decay

IRF_T = biological intake retention fraction

λ = radioactive decay constant

t = time after intake

Table 5.7: Intake Retention Fractions for the Lung

Days Post Intake	Cs-137	Co-60		Am-241	Ir-192			I-131	Sr-90/Y-90	
	F	M	S	M	F	M	S	F	F	S
0.25	0.264	0.326	0.333	0.326	0.263	0.325	0.332	0.258	0.264	0.333
0.50	0.205	0.265	0.272	0.265	0.204	0.264	0.271	0.196	0.205	0.272
0.75	0.160	0.219	0.225	0.219	0.159	0.217	0.223	0.150	0.160	0.225
1.00	0.125	0.182	0.189	0.182	0.124	0.180	0.187	0.115	0.125	0.189
1.25	0.097	0.154	0.161	0.154	0.096	0.152	0.159	0.087	0.097	0.161
1.50	0.075	0.132	0.139	0.132	0.074	0.130	0.137	0.066	0.075	0.139
1.75	0.059	0.115	0.122	0.115	0.058	0.113	0.120	0.051	0.059	0.122
2.00	0.046	0.102	0.109	0.102	0.045	0.100	0.107	0.039	0.046	0.109
2.25	0.036	0.091	0.098	0.091	0.035	0.090	0.096	0.029	0.036	0.098
2.50	0.028	0.083	0.090	0.083	0.027	0.081	0.088	0.022	0.028	0.090
2.75	0.022	0.077	0.084	0.077	0.021	0.075	0.082	0.017	0.022	0.084
3.00	0.017	0.072	0.079	0.072	0.016	0.070	0.077	0.013	0.017	0.079
4.00	0.006	0.061	0.068	0.061	0.006	0.058	0.065	0.004	0.006	0.068
5.00	0.002	0.056	0.063	0.056	0.002	0.053	0.060	0.001	0.002	0.063
6.00	0.001	0.053	0.061	0.054	0.001	0.051	0.058	0.001	0.001	0.061
7.00	3.1E-04	0.052	0.060	0.052	2.9E-04	0.049	0.056	1.7E-04	3.1E-04	0.060

From the IRF data the Minimum Detectable Intake (MDI) can be determined using Equation 5.3. The MDI and subsequent MDD are based on the MDA with a 10 minute counting time using the MIRD phantoms. The MDI for the various MIRD phantoms are shown in Tables 5.8-5.12. The last row in these tables list the MDA values

used to determine the respective MDI values. The errors associated with the IRF, half-life, and dose conversion coefficient data were assumed to be negligible. This means that the error in the MDI and MDD are the same as in Table 5.6 for each corresponding isotope and phantom model. The appendix shows the MDI and MDD for the LLNL phantom, which agrees well with that of the male MIRD phantom.

$$MDI = \frac{MDA}{IRF_R} \qquad [5.3]$$

Table 5.8: Minimum Detectable Intake for the Male MIRD Phantom (nCi)

Days Post Intake	Cs-137	Co-60		Am-241	Ir-192			I-131
	F	M	S	M	F	M	S	F
0.25	65.6	31.0	30.4	46.3	31.9	25.8	25.3	63.7
0.50	84.4	38.2	37.2	57.0	41.1	31.8	31.0	83.8
0.75	108.2	46.2	45.0	69.0	52.8	38.6	37.6	109.7
1.00	138.5	55.6	53.5	83.0	67.8	46.5	44.8	143.4
1.25	178.4	65.7	62.9	98.1	87.5	55.1	52.7	188.9
1.50	229.3	76.7	72.8	114.4	112.7	64.5	61.2	247.9
1.75	294.4	88.0	83.0	131.4	145.0	74.2	69.9	325.3
2.00	378.0	99.2	92.9	148.1	186.7	83.8	78.4	426.7
2.25	484.9	110.6	102.9	165.1	240.0	93.6	87.1	559.3
2.50	622.7	121.4	112.1	181.1	309.0	103.0	95.1	733.9
2.75	801.4	131.5	120.5	196.2	398.6	111.8	102.5	965.2
3.00	1024.3	140.6	128.2	209.8	510.6	119.9	109.2	1260.5
4.00	2792.3	167.2	149.6	249.3	1404.9	143.7	128.7	3745.3
5.00	7593.6	181.6	160.3	270.7	3856.4	157.6	139.1	1.1E+04
6.00	2.1E+04	189.1	165.6	281.8	1.1E+04	165.6	145.0	3.3E+04
7.00	5.6E+04	193.9	168.7	288.8	2.9E+04	171.3	149.1	9.7E+04
Based on 10 Minute MDA (nCi)	17.3	10.1	10.1	15.1	8.4	8.4	8.4	16.4

Table 5.9: Minimum Detectable Intake for the Female MIRD Phantom (nCi)

Days Post Intake	Cs-137	Co-60		Am-241	Ir-192			I-131
	F	M	S	M	F	M	S	F
0.25	53.5	25.4	24.9	38.7	26.3	21.3	20.8	52.1
0.50	68.9	31.3	30.5	47.6	33.9	26.2	25.6	68.6
0.75	88.3	37.8	36.8	57.6	43.6	31.8	31.0	89.8
1.00	113.1	45.5	43.9	69.3	55.9	38.4	37.0	117.4
1.25	145.7	53.8	51.5	81.9	72.2	45.5	43.5	154.6
1.50	187.2	62.8	59.6	95.6	93.0	53.2	50.5	203.0
1.75	240.4	72.1	68.0	109.7	119.7	61.2	57.7	266.3
2.00	308.6	81.3	76.1	123.7	154.0	69.1	64.7	349.3
2.25	395.9	90.6	84.3	137.9	198.0	77.3	71.8	457.9
2.50	508.4	99.4	91.8	151.3	254.9	85.0	78.5	600.8
2.75	654.3	107.7	98.7	163.8	328.8	92.2	84.5	790.1
3.00	836.3	115.2	105.0	175.2	421.2	98.9	90.1	1031.8
4.00	2279.8	136.9	122.6	208.2	1159.0	118.6	106.1	3065.8
5.00	6200.0	148.8	131.4	226.1	3181.3	130.0	114.8	9087.6
6.00	1.7E+04	154.9	135.7	235.4	8726.7	136.6	119.6	2.7E+04
7.00	4.6E+04	158.8	138.2	241.2	2.4E+04	141.3	123.0	8.0E+04
Based on 10 Minute MDA (nCi)	14.1	8.3	8.3	12.6	6.9	6.9	6.9	13.5

Table 5.10: Minimum Detectable Intake for the Adipose Male MIRD Phantom (nCi)

Days Post Intake	Cs-137	Co-60		Am-241	Ir-192			I-131
	F	M	S	M	F	M	S	F
0.25	171.8	72.9	71.4	140.6	82.0	66.4	65.0	179.4
0.50	221.3	89.7	87.4	172.9	105.9	81.9	79.8	236.0
0.75	283.6	108.6	105.7	209.3	136.0	99.3	96.7	309.0
1.00	363.0	130.7	125.8	251.8	174.4	119.8	115.4	404.1
1.25	467.7	154.5	147.7	297.6	225.3	141.9	135.8	532.2
1.50	600.9	180.2	171.1	347.2	290.2	166.0	157.6	698.6
1.75	771.6	206.9	195.0	398.5	373.5	190.9	180.0	916.6
2.00	990.7	233.3	218.3	449.3	480.6	215.8	201.9	1202.3
2.25	1271.0	260.0	241.8	500.9	618.0	241.1	224.2	1576.1
2.50	1632.2	285.3	263.5	549.5	795.5	265.2	244.9	2068.1
2.75	2100.7	309.1	283.3	595.2	1026.2	287.9	263.9	2719.7
3.00	2685.0	330.6	301.3	636.6	1314.6	308.6	281.2	3551.8
4.00	7319.2	392.9	351.7	756.3	3617.2	370.1	331.3	1.1E+04
5.00	2.0E+04	426.8	376.9	821.4	9928.8	405.7	358.2	3.1E+04
6.00	5.4E+04	444.5	389.3	855.1	2.7E+04	426.3	373.4	9.3E+04
7.00	1.5E+05	455.7	396.6	876.3	7.5E+04	441.0	383.8	2.7E+05
Based on 10 Minute MDA (nCi)	45.4	23.8	23.8	45.8	21.6	21.6	21.6	46.3

Table 5.11: Minimum Detectable Intake for the Adipose Female MIRD Phantom (nCi)

Days Post Intake	Cs-137	Co-60		Am-241	Ir-192			I-131
	F	M	S	M	F	M	S	F
0.25	147.8	61.8	60.5	124.2	70.7	57.3	56.0	151.5
0.50	190.3	76.0	74.0	152.8	91.3	70.6	68.8	199.4
0.75	243.8	92.0	89.5	184.9	117.2	85.6	83.3	261.0
1.00	312.1	110.7	106.6	222.5	150.4	103.3	99.4	341.4
1.25	402.2	130.8	125.1	262.9	194.2	122.3	117.0	449.6
1.50	516.8	152.6	144.9	306.7	250.1	143.1	135.9	590.2
1.75	663.5	175.2	165.1	352.1	321.9	164.6	155.1	774.3
2.00	851.9	197.5	184.9	397.0	414.2	186.0	174.1	1015.7
2.25	1092.9	220.2	204.8	442.5	532.7	207.8	193.3	1331.5
2.50	1403.5	241.6	223.2	485.5	685.7	228.6	211.1	1747.1
2.75	1806.4	261.8	239.9	525.9	884.5	248.1	227.5	2297.6
3.00	2308.9	280.0	255.1	562.4	1133.2	266.0	242.4	3000.5
4.00	6293.9	332.7	297.8	668.2	3117.9	319.0	285.5	8915.2
5.00	1.7E+04	361.5	319.2	725.6	8558.3	349.7	308.7	2.6E+04
6.00	4.7E+04	376.5	329.7	755.4	2.3E+04	367.5	321.8	7.8E+04
7.00	1.3E+05	386.0	335.9	774.2	6.4E+04	380.2	330.8	2.3E+05
Based on 10 Minute MDA (nCi)	39.0	20.1	20.1	40.5	18.6	18.6	18.6	39.2

Table 5.12: Minimum Detectable Intake for the Child MIRD Phantom (nCi)

Days Post Intake	Cs-137	Co-60		Am-241	Ir-192			I-131
	F	M	S	M	F	M	S	F
0.25	48.0	22.9	22.4	34.3	23.5	19.0	18.6	46.7
0.50	61.8	28.2	27.5	42.2	30.3	23.5	22.8	61.4
0.75	79.2	34.1	33.2	51.0	38.9	28.4	27.7	80.4
1.00	101.3	41.1	39.6	61.4	49.9	34.3	33.0	105.2
1.25	130.6	48.6	46.4	72.5	64.5	40.6	38.9	138.5
1.50	167.8	56.6	53.8	84.6	83.1	47.5	45.1	181.8
1.75	215.4	65.0	61.3	97.2	106.9	54.7	51.5	238.6
2.00	276.6	73.3	68.6	109.5	137.6	61.8	57.8	313.0
2.25	354.8	81.7	76.0	122.1	176.9	69.0	64.2	410.3
2.50	455.7	89.7	82.8	134.0	227.8	75.9	70.1	538.3
2.75	586.5	97.2	89.1	145.1	293.8	82.4	75.6	707.9
3.00	749.6	103.9	94.7	155.2	376.4	88.4	80.5	924.5
4.00	2043.4	123.5	110.6	184.4	1035.7	106.0	94.9	2746.9
5.00	5557.0	134.2	118.5	200.2	2842.9	116.2	102.6	8142.3
6.00	1.5E+04	139.7	122.4	208.4	7798.4	122.1	106.9	2.4E+04
7.00	4.1E+04	143.3	124.7	213.6	2.1E+04	126.3	109.9	7.1E+04
Based on 10 Minute MDA (nCi)	12.7	7.5	7.5	11.2	6.2	6.2	6.2	12.1

After obtaining the MDI, the MDD can be calculated using Dose Conversion Coefficients (DCC). The inhalation values using the Committed Effective Dose Equivalent (CEDE) were reported by the Environmental Protection Agency and are derived from data in ICRP Publication 26 (EPA, 1998; ICRP, 1977). The Committed Effective Dose (CED) values are from ICRP Publication 60 (ICRP, 1991). The dose values obtained from both of these conversion factors is the effective dose experienced by a person after a 50 year period after inhalation. The DCC values are shown in Table 5.13. ICRP 60 uses different tissue weighting factors than ICRP 26. Publication 60 also uses radiation weighting factors instead of the previously used quality factors. It should be noted that the DCC of ^{241}Am is several orders of magnitude higher than for any of the other isotopes. This is due to the fact that ^{241}Am is an alpha emitter.

Table 5.13: Dose Conversion Coefficients (mrem/nCi)

Radioisotope	Particle Class	CEDE (ICRP 26)	CED (ICRP 60)	CED (ICRP 60)
		Adult	Adult	10-yr-old
Cs-137	F	0.032	0.017	0.014
Co-60	M	0.033	0.037	0.056
	S	0.219	0.115	0.148
Am-241	M	444.0	156.0	148.0
Ir-192	F	0.019	0.007	0.012
	M	0.018	0.019	0.028
	S	0.028	0.024	0.035
I-131	F	0.033	0.027	0.070
Sr-90/Y-90	F	0.239	0.089	0.152
	S	1.299	0.593	0.667

The MDD can now be calculated using Equation 5.4. The MDD values calculated at several different times post exposure using both ICRP 26 and 60 conversion factors are shown in Tables 5.14-5.23 and are reported in mrem.

$$MDD = MDI \times DCC \quad [5.4]$$

Table 5.14: MDD for the Male MIRD Phantom (CEDE) (ICRP 26) (mrem)

Days Post	Cs-137	Co-60		Am-241	Ir-192			I-131
Intake	F	M	S	M	F	M	S	F
0.25	2.09	1.03	6.64	2.06E+04	0.60	0.47	0.71	2.09
0.50	2.70	1.26	8.13	2.53E+04	0.78	0.57	0.87	2.76
0.75	3.45	1.53	9.83	3.06E+04	1.00	0.70	1.06	3.61
1.00	4.42	1.84	11.71	3.69E+04	1.28	0.84	1.26	4.72
1.25	5.70	2.17	13.74	4.36E+04	1.65	1.00	1.48	6.21
1.50	7.32	2.54	15.9	5.08E+04	2.13	1.16	1.72	8.16
1.75	9.40	2.91	18.1	5.83E+04	2.74	1.34	1.97	10.70
2.00	12.07	3.28	20.3	6.58E+04	3.52	1.51	2.21	14.04
2.25	15.5	3.66	22.5	7.33E+04	4.53	1.69	2.45	18.4
2.50	19.9	4.02	24.5	8.04E+04	5.83	1.86	2.68	24.1
2.75	25.6	4.35	26.4	8.71E+04	7.52	2.02	2.89	31.7
3.00	32.7	4.65	28.0	9.32E+04	9.64	2.16	3.08	41.5
4.00	89.2	5.53	32.7	1.11E+05	26.5	2.60	3.62	123.2
5.00	242	6.01	35.1	1.20E+05	72.8	2.85	3.92	365
6.00	659	6.26	36.2	1.25E+05	200	2.99	4.08	1082
7.00	1789	6.41	36.9	1.28E+05	547	3.09	4.20	3201

Table 5.15: MDD for the Male MIRD Phantom (CED) (ICRP 60) (mrem)

Days Post	Cs-137	Co-60		Am-241	Ir-192			I-131
Intake	F	M	S	M	F	M	S	F
0.25	1.11	1.15	3.49	7.23E+03	0.21	0.50	0.62	1.74
0.50	1.44	1.41	4.28	8.89E+03	0.27	0.61	0.76	2.30
0.75	1.84	1.71	5.17	1.08E+04	0.35	0.74	0.92	3.00
1.00	2.35	2.06	6.16	1.29E+04	0.45	0.90	1.09	3.93
1.25	3.03	2.43	7.23	1.53E+04	0.58	1.06	1.29	5.17
1.50	3.90	2.84	8.37	1.79E+04	0.75	1.24	1.49	6.79
1.75	5.00	3.26	9.54	2.05E+04	0.97	1.43	1.71	8.91
2.00	6.43	3.67	10.68	2.31E+04	1.24	1.62	1.91	11.69
2.25	8.24	4.09	11.83	2.58E+04	1.60	1.81	2.12	15.3
2.50	10.59	4.49	12.89	2.83E+04	2.06	1.99	2.32	20.1
2.75	13.62	4.87	13.86	3.06E+04	2.66	2.16	2.50	26.4
3.00	17.4	5.20	14.74	3.27E+04	3.41	2.31	2.67	34.5
4.00	47.5	6.18	17.2	3.89E+04	9.37	2.77	3.14	102.6
5.00	129.1	6.72	18.4	4.22E+04	25.7	3.04	3.39	304
6.00	351	7.00	19.0	4.40E+04	70.6	3.20	3.54	901
7.00	953	7.17	19.4	4.51E+04	193	3.31	3.64	2667

Table 5.16: MDD for the Female MIRD Phantom (CEDE) (ICRP 26) (mrem)

Days Post	Cs-137	Co-60		Am-241	Ir-192			I-131
Intake	F	M	S	M	F	M	S	F
0.25	1.71	0.84	5.44	1.72E+04	0.50	0.38	0.59	1.71
0.50	2.20	1.03	6.66	2.11E+04	0.64	0.47	0.72	2.26
0.75	2.82	1.25	8.06	2.56E+04	0.82	0.57	0.87	2.95
1.00	3.61	1.51	9.59	3.08E+04	1.05	0.69	1.04	3.86
1.25	4.65	1.78	11.26	3.64E+04	1.36	0.82	1.22	5.09
1.50	5.98	2.08	13.04	4.24E+04	1.75	0.96	1.42	6.68
1.75	7.67	2.39	14.86	4.87E+04	2.26	1.10	1.62	8.76
2.00	9.85	2.69	16.6	5.49E+04	2.91	1.25	1.82	11.49
2.25	12.64	3.00	18.4	6.12E+04	3.74	1.39	2.02	15.1
2.50	16.2	3.29	20.1	6.72E+04	4.81	1.53	2.21	19.8
2.75	20.9	3.56	21.6	7.27E+04	6.20	1.67	2.38	26.0
3.00	26.7	3.81	23.0	7.78E+04	7.95	1.79	2.54	33.9
4.00	72.8	4.53	26.8	9.24E+04	21.9	2.14	2.99	100.8
5.00	198	4.92	28.7	1.00E+05	60.0	2.35	3.23	299
6.00	538	5.12	29.7	1.05E+05	165	2.47	3.37	885
7.00	1461	5.25	30.2	1.07E+05	451	2.55	3.46	2621

Table 5.17: MDD for the Female MIRD Phantom (CED) (ICRP 60) (mrem)

Days Post	Cs-137	Co-60		Am-241	Ir-192			I-131
Intake	F	M	S	M	F	M	S	F
0.25	0.91	0.94	2.86	6.04E+03	0.18	0.41	0.51	1.43
0.50	1.17	1.16	3.50	7.43E+03	0.23	0.51	0.62	1.88
0.75	1.50	1.40	4.24	8.99E+03	0.29	0.61	0.76	2.46
1.00	1.92	1.69	5.04	1.08E+04	0.37	0.74	0.90	3.22
1.25	2.48	1.99	5.92	1.28E+04	0.48	0.88	1.06	4.24
1.50	3.18	2.32	6.86	1.49E+04	0.62	1.03	1.23	5.56
1.75	4.09	2.67	7.82	1.71E+04	0.80	1.18	1.41	7.30
2.00	5.25	3.01	8.75	1.93E+04	1.03	1.33	1.58	9.57
2.25	6.73	3.35	9.69	2.15E+04	1.32	1.49	1.75	12.55
2.50	8.64	3.68	10.56	2.36E+04	1.70	1.64	1.91	16.5
2.75	11.12	3.99	11.36	2.56E+04	2.19	1.78	2.06	21.6
3.00	14.22	4.26	12.08	2.73E+04	2.81	1.91	2.20	28.3
4.00	38.8	5.07	14.10	3.25E+04	7.73	2.29	2.59	84.0
5.00	105.4	5.50	15.1	3.53E+04	21.2	2.51	2.80	249
6.00	286	5.73	15.6	3.67E+04	58.2	2.64	2.92	738
7.00	778	5.88	15.9	3.76E+04	160	2.73	3.00	2183

Table 5.18: MDD for the Adipose Male MIRD Phantom (CEDE) (ICRP 26) (mrem)

Days Post	Cs-137	Co-60		Am-241	Ir-192			I-131
Intake	F	M	S	M	F	M	S	F
0.25	0.91	0.94	2.86	6.04E+03	0.18	0.41	0.51	1.43
0.50	1.17	1.16	3.50	7.43E+03	0.23	0.51	0.62	1.88
0.75	1.50	1.40	4.24	8.99E+03	0.29	0.61	0.76	2.46
1.00	1.92	1.69	5.04	1.08E+04	0.37	0.74	0.90	3.22
1.25	2.48	1.99	5.92	1.28E+04	0.48	0.88	1.06	4.24
1.50	3.18	2.32	6.86	1.49E+04	0.62	1.03	1.23	5.56
1.75	4.09	2.67	7.82	1.71E+04	0.80	1.18	1.41	7.30
2.00	5.25	3.01	8.75	1.93E+04	1.03	1.33	1.58	9.57
2.25	6.73	3.35	9.69	2.15E+04	1.32	1.49	1.75	12.55
2.50	8.64	3.68	10.56	2.36E+04	1.70	1.64	1.91	16.5
2.75	11.12	3.99	11.36	2.56E+04	2.19	1.78	2.06	21.6
3.00	14.22	4.26	12.08	2.73E+04	2.81	1.91	2.20	28.3
4.00	38.8	5.07	14.10	3.25E+04	7.73	2.29	2.59	84.0
5.00	105.4	5.50	15.1	3.53E+04	21.2	2.51	2.80	249
6.00	286	5.73	15.6	3.67E+04	58.2	2.64	2.92	738
7.00	778	5.88	15.9	3.76E+04	160	2.73	3.00	2183

Table 5.19: MDD for the Adipose Male MIRD Phantom (CED) (ICRP 60) (mrem)

Days Post	Cs-137	Co-60		Am-241	Ir-192			I-131
Intake	F	M	S	M	F	M	S	F
0.25	2.92	2.70	8.21	2.19E+04	0.55	1.28	1.59	4.91
0.50	3.76	3.32	10.05	2.70E+04	0.71	1.58	1.95	6.47
0.75	4.82	4.02	12.15	3.26E+04	0.91	1.92	2.36	8.47
1.00	6.17	4.84	14.47	3.93E+04	1.16	2.31	2.82	11.07
1.25	7.95	5.71	17.0	4.64E+04	1.50	2.74	3.31	14.58
1.50	10.22	6.67	19.7	5.42E+04	1.94	3.20	3.85	19.1
1.75	13.12	7.65	22.4	6.22E+04	2.49	3.69	4.39	25.1
2.00	16.8	8.63	25.1	7.01E+04	3.21	4.16	4.93	32.9
2.25	21.6	9.62	27.8	7.81E+04	4.12	4.65	5.47	43.2
2.50	27.7	10.56	30.3	8.57E+04	5.31	5.12	5.98	56.7
2.75	35.7	11.44	32.6	9.29E+04	6.84	5.56	6.44	74.5
3.00	45.6	12.23	34.6	9.93E+04	8.77	5.96	6.86	97.3
4.00	124.4	14.54	40.4	1.18E+05	24.1	7.14	8.08	289
5.00	338	15.8	43.3	1.28E+05	66.2	7.83	8.74	857
6.00	920	16.4	44.8	1.33E+05	182	8.23	9.11	2539
7.00	2497	16.9	45.6	1.37E+05	498	8.51	9.36	7514

Table 5.20: MDD for the Adipose Female MIRD Phantom (CEDE) (ICRP 26) (mrem)

Days Post	Cs-137	Co-60		Am-241	Ir-192			I-131
Intake	F	M	S	M	F	M	S	F
0.25	4.72	2.04	13.22	5.51E+04	1.33	1.03	1.58	4.98
0.50	6.08	2.51	16.2	6.78E+04	1.72	1.27	1.94	6.56
0.75	7.79	3.04	19.6	8.21E+04	2.21	1.55	2.35	8.59
1.00	9.97	3.66	23.3	9.88E+04	2.84	1.86	2.80	11.23
1.25	12.84	4.33	27.4	1.17E+05	3.66	2.21	3.29	14.79
1.50	16.5	5.05	31.7	1.36E+05	4.72	2.58	3.83	19.4
1.75	21.2	5.80	36.1	1.56E+05	6.07	2.97	4.37	25.5
2.00	27.2	6.53	40.4	1.76E+05	7.82	3.36	4.90	33.4
2.25	34.9	7.28	44.8	1.96E+05	10.05	3.75	5.44	43.8
2.50	44.8	7.99	48.8	2.16E+05	12.94	4.13	5.94	57.5
2.75	57.7	8.66	52.5	2.33E+05	16.7	4.48	6.40	75.6
3.00	73.7	9.26	55.8	2.50E+05	21.4	4.80	6.83	98.7
4.00	201	11.01	65.1	2.97E+05	58.8	5.76	8.04	293
5.00	547	11.96	69.8	3.22E+05	161	6.31	8.69	869
6.00	1485	12.45	72.1	3.35E+05	443	6.64	9.06	2575
7.00	4033	12.77	73.4	3.44E+05	1214	6.86	9.31	7621

Table 5.21: MDD for the Adipose Female MIRD Phantom (CED) (ICRP 60) (mrem)

Days Post	Cs-137	Co-60		Am-241	Ir-192			I-131
Intake	F	M	S	M	F	M	S	F
0.25	2.51	2.29	6.95	1.94E+04	0.47	1.10	1.37	4.15
0.50	3.24	2.81	8.51	2.38E+04	0.61	1.36	1.68	5.46
0.75	4.15	3.40	10.29	2.88E+04	0.78	1.65	2.03	7.15
1.00	5.31	4.09	12.26	3.47E+04	1.00	1.99	2.43	9.35
1.25	6.84	4.84	14.39	4.10E+04	1.30	2.36	2.86	12.32
1.50	8.79	5.65	16.7	4.79E+04	1.67	2.76	3.31	16.2
1.75	11.28	6.48	19.0	5.49E+04	2.15	3.18	3.79	21.2
2.00	14.48	7.31	21.3	6.19E+04	2.76	3.59	4.25	27.8
2.25	18.6	8.15	23.6	6.90E+04	3.55	4.01	4.72	36.5
2.50	23.9	8.94	25.7	7.57E+04	4.57	4.41	5.15	47.9
2.75	30.7	9.68	27.6	8.20E+04	5.90	4.79	5.55	63.0
3.00	39.3	10.36	29.3	8.77E+04	7.56	5.13	5.91	82.2
4.00	107.0	12.31	34.3	1.04E+05	20.8	6.16	6.97	244
5.00	291	13.38	36.7	1.13E+05	57.1	6.75	7.53	724
6.00	791	13.93	37.9	1.18E+05	157	7.09	7.85	2145
7.00	2147	14.28	38.6	1.21E+05	429	7.34	8.07	6348

Table 5.22: MDD for the Child MIRD Phantom (CEDE) (ICRP 26) (mrem)

Days Post	Cs-137	Co-60		Am-241	Ir-192			I-131
Intake	F	M	S	M	F	M	S	F
0.25	1.53	0.76	4.91	1.52E+04	0.44	0.34	0.52	1.54
0.50	1.97	0.93	6.01	1.87E+04	0.57	0.42	0.64	2.02
0.75	2.53	1.13	7.27	2.27E+04	0.73	0.51	0.78	2.65
1.00	3.24	1.36	8.65	2.73E+04	0.94	0.62	0.93	3.46
1.25	4.17	1.61	10.16	3.22E+04	1.22	0.73	1.09	4.56
1.50	5.36	1.87	11.76	3.76E+04	1.57	0.86	1.27	5.98
1.75	6.88	2.15	13.40	4.31E+04	2.02	0.99	1.45	7.85
2.00	8.83	2.43	15.0	4.86E+04	2.60	1.12	1.63	10.29
2.25	11.33	2.70	16.6	5.42E+04	3.34	1.25	1.81	13.49
2.50	14.55	2.97	18.1	5.95E+04	4.30	1.37	1.97	17.7
2.75	18.7	3.21	19.5	6.44E+04	5.54	1.49	2.13	23.3
3.00	23.9	3.44	20.7	6.89E+04	7.10	1.60	2.27	30.4
4.00	65.2	4.09	24.2	8.19E+04	19.5	1.91	2.67	90.4
5.00	177	4.44	25.9	8.89E+04	53.6	2.10	2.89	268
6.00	482	4.62	26.8	9.26E+04	147.2	2.20	3.01	793
7.00	1309	4.74	27.3	9.49E+04	403	2.28	3.09	2348

Table 5.23: MDD for the Child MIRD Phantom (CED) (ICRP 60) (mrem)

Days Post	Cs-137	Co-60		Am-241	Ir-192			I-131
Intake	F	M	S	M	F	M	S	F
0.25	0.66	1.27	3.32	5.07E+03	0.29	0.53	0.66	3.29
0.50	0.85	1.57	4.07	6.24E+03	0.37	0.66	0.80	4.33
0.75	1.08	1.90	4.92	7.55E+03	0.47	0.80	0.97	5.66
1.00	1.39	2.28	5.85	9.09E+03	0.61	0.96	1.16	7.41
1.25	1.79	2.70	6.87	1.07E+04	0.79	1.14	1.37	9.75
1.50	2.30	3.15	7.96	1.25E+04	1.01	1.34	1.59	12.80
1.75	2.95	3.62	9.07	1.44E+04	1.30	1.54	1.81	16.8
2.00	3.79	4.08	10.16	1.62E+04	1.68	1.74	2.04	22.0
2.25	4.86	4.55	11.25	1.81E+04	2.16	1.94	2.26	28.9
2.50	6.24	4.99	12.26	1.98E+04	2.78	2.13	2.47	37.9
2.75	8.03	5.40	13.18	2.15E+04	3.58	2.32	2.66	49.8
3.00	10.27	5.78	14.02	2.30E+04	4.59	2.48	2.83	65.1
4.00	28.0	6.87	16.4	2.73E+04	12.64	2.98	3.34	193
5.00	76.1	7.46	17.5	2.96E+04	34.7	3.26	3.61	573
6.00	207	7.77	18.1	3.09E+04	95.1	3.43	3.76	1698
7.00	562	7.97	18.5	3.16E+04	261	3.55	3.87	5026

For ^{241}Am the bone surface dose will be much higher than the effective dose. The CEDE (ICRP 26) and CED (ICRP 60) conversion coefficients are 8.03 rem/nCi and 6.30 rem/nCi respectively. These will lead to the MDD values shown in Table 5.24.

Table 5.24: MDD to the Bone Surface for ^{241}Am (rem)

Phantom	Days Post Intake	0.25	1.00	2.00	3.00	5.00	7.00
Male	CEDE (ICRP 26)	3.7E+02	6.7E+02	1.2E+03	1.7E+03	2.2E+03	2.3E+03
	CED (ICRP 60)	2.9E+02	5.2E+02	9.3E+02	1.3E+03	1.7E+03	1.8E+03
Female	CEDE (ICRP 26)	3.1E+02	5.6E+02	9.9E+02	1.4E+03	1.8E+03	1.9E+03
	CED (ICRP 60)	2.4E+02	4.4E+02	7.8E+02	1.1E+03	1.4E+03	1.5E+03
Adipose Male	CEDE (ICRP 26)	1.1E+03	2.0E+03	3.6E+03	5.1E+03	6.6E+03	7.0E+03
	CED (ICRP 60)	8.9E+02	1.6E+03	2.8E+03	4.0E+03	5.2E+03	5.5E+03
Adipose Female	CEDE (ICRP 26)	1.0E+03	1.8E+03	3.2E+03	4.5E+03	5.8E+03	6.2E+03
	CED (ICRP 60)	7.8E+02	1.4E+03	2.5E+03	3.5E+03	4.6E+03	4.9E+03
Child	CEDE (ICRP 26)	2.8E+02	4.9E+02	8.8E+02	1.2E+03	1.6E+03	1.7E+03
	CED (ICRP 60)	2.2E+02	3.9E+02	6.9E+02	9.8E+02	1.3E+03	1.3E+03

It can be seen from the tables above that the MDD for ^{241}Am is much larger than for all of the other isotopes. This very large MDD means that using this detector to measure ^{241}Am inhaled by a victim of an RDD would not be feasible under most circumstances. For the other isotopes considered, the MDD is fairly low. As long as the analysis happens within four days, the MDD will always be below 1 rem.

Strontium/Yttrium

Secondary photons created by the radioisotope ^{90}Sr were also looked at. This isotope undergoes beta decay with a half-life of 28.79 years. When an isotope undergoes beta decay, a neutron is converted into a proton and an electron is ejected. So ^{90}Sr will decay into ^{90}Y, which then decays into ^{90}Zr, which is a stable isotope. The isotope ^{90}Y has a half-life of 64 hours. When a parent nuclide has a much longer half-life than its

daughter, the two isotopes are assumed to be in secular equilibrium (both have equal activities) after seven daughter half-lives. It was assumed for this work that the isotopes are in secular equilibrium. The maximum electron energy emitted in a beta decay is 500 keV for ^{90}Sr and 2.2 MeV for ^{90}Y.

A computational model of the male MIRD phantom with a ^{90}Sr/^{90}Y source was run. This was the only model run because electron transport requires more computations than photons. Electron transport was only considered inside the lungs (the importance in all of the other cells was set to zero). This was done to speed up computational time. Figures 5.1-5.2 shows the electron spectrum of ^{90}Sr/^{90}Y used in the MCNP input and the photon spectrum tallied by the detector in MCNP. If this spectrum was observed on actual patients, it would not be possible to identify the radionuclide because there is no gamma peak. This is not of concern for this application though, since the isotope used in an RDD would be determined before scanning patients.

The energy range that was integrated over in determining the efficiency was the entire range of the detector (up to 1.5 MeV). The efficiency obtained for this model was $7x10^{-5}\pm5x10^{-7}$, nearly an order of magnitude lower than for all of the other isotopes studied. This is expected since many electrons will not create bremsstrahlung photons. The MDA data for the male MIRD phantom are shown in Table 5.25 and have an uncertainty of 1.2%.

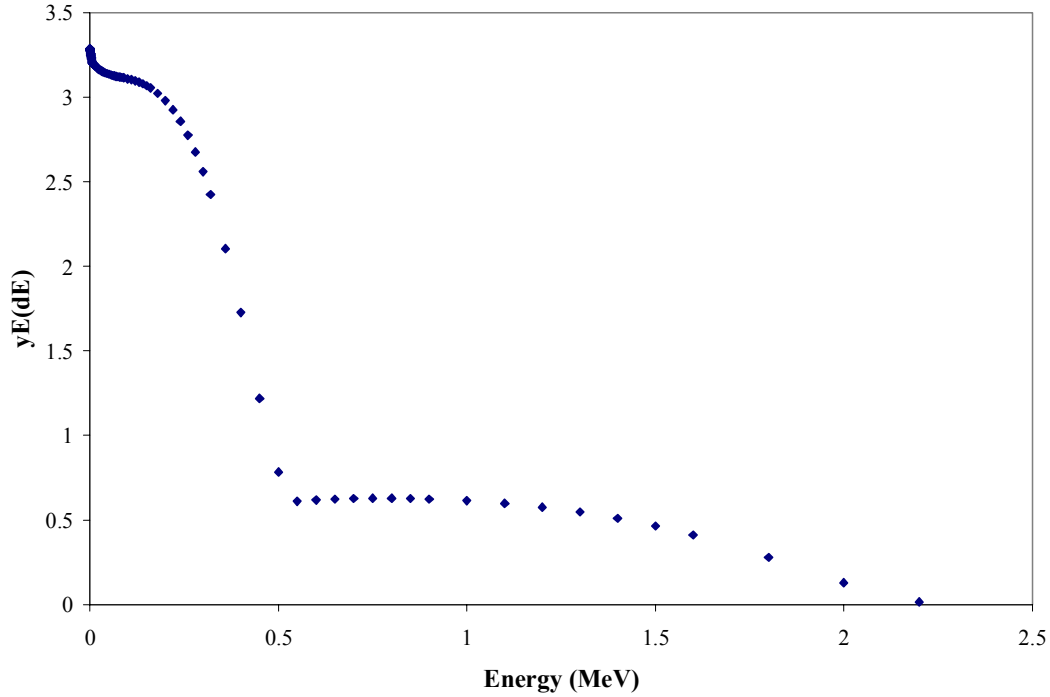

Figure 5.1: Electron Spectrum for $^{90}Sr/^{90}Y$

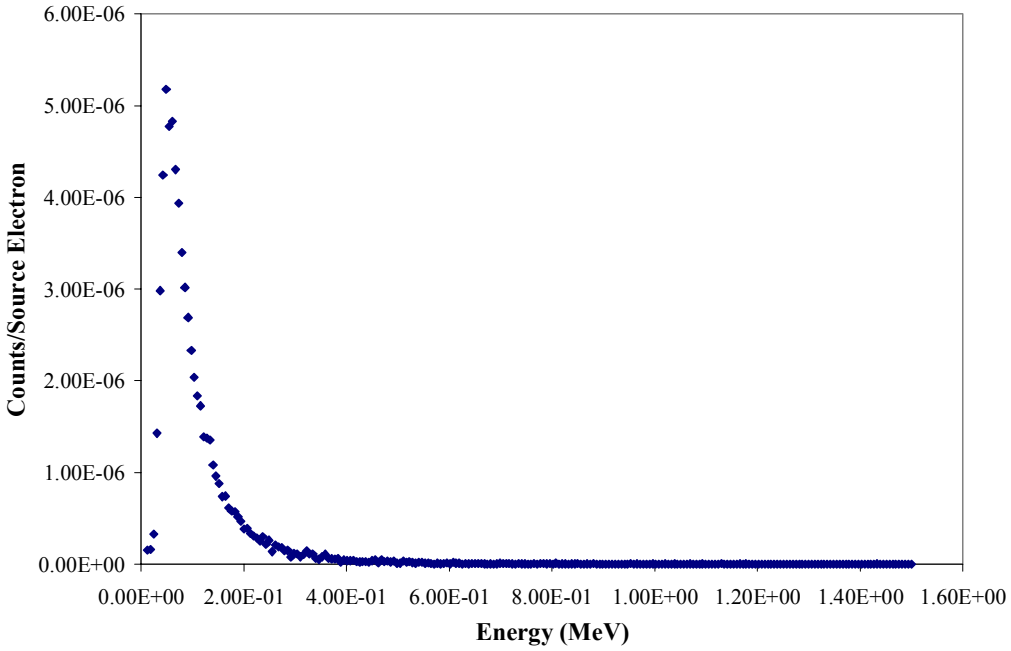

Figure 5.2: Photon Spectrum for $^{90}Sr/^{90}Y$

Table 5.25: MDA for $^{90}Sr/^{90}Y$ in the Male MIRD Phantom

Counting Time (Minutes)	MDA (μCi)
1	1.7
5	0.7
10	0.5

As observed with the efficiency, the MDA is also much higher for $^{90}Sr/^{90}Y$ than the other isotopes studied. The MDI and MDD for $^{90}Sr/^{90}Y$ based on ten-minute counting times are shown in Table 5.26.

Table 5.26: MDI and MDD for $^{90}Sr/^{90}Y$ in the Male MIRD Phantom

Days Post Intake	MDI (μCi)		MDD (mrem) using CEDE		MDD (mrem) using CED	
	Type F	Type S	Type F	Type S	Type F	Type S
0.25	2.1	1.6	493	2121	183	968
0.50	2.7	2.0	635	2597	236	1186
0.75	3.4	2.4	814	3139	302	1433
1.00	4.4	2.9	1042	3737	387	1706
1.25	5.6	3.4	1342	4387	498	2003
1.50	7.2	3.9	1725	5082	640	2320
1.75	9.2	4.5	2214	5790	822	2644
2.00	11.9	5.0	2843	6480	1056	2959
2.25	15.2	5.5	3647	7179	1354	3278
2.50	19.6	6.0	4684	7823	1739	3572
2.75	25.2	6.5	6028	8410	2239	3840
3.00	32.2	6.9	7705	8942	2861	4083
4.00	87.7	8.0	2.1E+04	1.0E+04	7800	4765
5.00	238.6	8.6	5.7E+04	1.1E+04	2.1E+04	5104
6.00	648.5	8.9	1.6E+05	1.2E+04	5.8E+04	5272
7.00	1760.8	9.1	4.2E+05	1.2E+04	1.6E+05	5368

The MDD for $^{90}Sr/^{90}Y$ is much higher than all of the other isotopes excluding ^{241}Am. It is still possible to detect $^{90}Sr/^{90}Y$, but counting should be performed very quickly after inhalation to achieve lower MDDs.

Background Spectrum Effects

The ambient background radiation levels used for this work were measured at a laboratory at Georgia Institute of Technology. This background spectrum could differ greatly from that at a site used to measure patients. The total background count rate at the laboratory was approximately 12,000 counts per minute. The background rate contained in the ROI of each isotope is shown below (Table 5.27).

Table 5.27 Background Count Rates

Radioisotope	ROI (keV)	Background (cpm)
Cs-137	601-723	277 ± 17
Co-60	1075-1427	223 ± 15
Am-241	36-73	993 ± 32
Ir-192	267-650	1314 ± 36
I-131	322-407	779 ± 28
Total	0-1.5 MeV	12037 ± 110

Since the background could be very different and this will significantly affect the MDA, different background spectrums were studied. Background rate multipliers were used to determine the effect on the MDA. The ratio of the MDA at a new background to the MDA at the original measured background varies very little for the different isotopes studied. All of the curves closely follow the curve described by:

$$y = -0.037x^2 + 0.530x + 0.479 \quad [5.4]$$

where:

x = background multiplication factor

y = MDA multiplication factor

Equation 5.4 applies for a background multiplication factor between the values of 0.5 and 5 (100-1000 total cps). From this equation, the ratio of the new background to the rate listed in Table 5.27 is plugged in for x. Then the MDA value listed in Table 5.6 for the isotope and phantom being considered is multiplied by y. This will approximate the MDA using the new background spectrum.

Tissue Thickness Determination

The tissue thicknesses between the lungs and the skin of a person will play a role in determining the amount of scattering present. As a person's tissue thickness increases, the counts in the photopeak region decrease but the number of counts recorded at lower energies increase. For these reasons, the peak counts divided by the total counts was computed for all of the phantoms used (Table 5.28 and Table 5.29). The tissue thickness listed in Table 5.28 is the tissue thickness from the center of the lung to the outside of the body where the detector is centered over. The ROIs for determining the photopeak counts are the same as in Table 4.1. These data might possibly be used to determine the inhaled activity for people with differing tissue thicknesses. It should be noted that the ^{241}Am data are probably not as reliable as the data for other radionuclides in this study. Since ^{241}Am only has one low-energy gamma (59.5 keV), the only non-zero channels that

are not located in the ROI are the lowest four energy channels. The detector would probably not give accurate readings at such low energies. For ^{241}Am it would probably be better to just look at the efficiency for the different models as shown in Table 5.4.

Table 5.28: Ratio of Peak Counts to Total Counts for the MIRD Phantoms

Phantom	Tissue Thickness (cm)	Cs-137	Co-60	Am-241	Ir-192	I-131
M MIRD	9.26	0.140	0.115	0.858	0.285	0.216
F MIRD	9.06	0.143	0.117	0.861	0.287	0.219
AM MIRD	14.31	0.084	0.074	0.839	0.188	0.129
AF MIRD	14.16	0.086	0.077	0.840	0.192	0.134
C MIRD	7.71	0.149	0.122	0.855	0.298	0.227

Table 5.29: Ratio of Peak Counts to Total Counts for the Slab Phantom

Slab Thickness (cm)	Peak Counts/Total Counts				
	Cs-137	Co-60	Am-241	Ir-192	I-131
0.0	0.190	0.149	0.869	0.338	0.281
0.5	0.178	0.141	0.863	0.318	0.261
1.0	0.166	0.132	0.859	0.300	0.244
1.5	0.157	0.125	0.856	0.285	0.230
2.0	0.147	0.119	0.853	0.272	0.217
2.5	0.138	0.113	0.851	0.259	0.204
3.0	0.131	0.107	0.847	0.248	0.194
4.0	0.119	0.099	0.841	0.228	0.175
5.0	0.108	0.092	0.836	0.212	0.160
7.5	0.087	0.076	0.822	0.181	0.130
10.0	0.072	0.066	0.807	0.155	0.106
13.8	0.053	0.050	0.798	0.123	0.079

CHAPTER 6

CONCLUSIONS

The purpose of this work was to determine if a handheld detector could be used to measure the radioactivity levels in lungs inhaled by a victim of an RDD. To determine this, measurements were made using the GR-130 with a slab phantom. Computational models were created for various isotopes utilizing both the slab phantom and anthropomorphic phantoms. The measured and calculated efficiencies for the slab phantom agreed within 6%. A voxel model was made of the LLNL phantom using Scan2MCNP. Five different MIRD phantom models were made using the BodyBuilder program.

The computed detector efficiency in the photopeak ROI for the GR-130 was generally between 0.05% and 0.4% using any of the primary gamma-emitting isotopes for the male MIRD phantom and LLNL voxel phantom. This led to MDA values ranging from approximately 5 to 150 nCi. From these MDA's, MDD values were calculated at a number of different elapsed times after intake up to one week. It was found that this detector could be used to triage patients for all of the isotopes studied except Am^{241}. Counting should be performed quickly after inhalation to obtain a low MDD when measuring bremsstrahlung photons from $^{90}Sr/^{90}Y$. The ambient background radiation levels at the measurement site after an RDD event could be different from the background data used in this work, so the effect of the background radiation level on the MDA was studied.

APPENDIX A

ADDITIONAL SLAB PHANTOM DATA

Table A.1: MDA Uncertainty for the Slab Model

Slab Thickness (cm)	MDA Uncertainty (%)				
	Cs-137	Co-60	Am-241	Ir-192	I-131
0.0	6.10	6.83	3.20	2.85	3.66
0.5	6.10	6.84	3.20	2.85	3.67
1.0	6.11	6.84	3.20	2.85	3.67
1.5	6.11	6.84	3.20	2.85	3.68
2.0	6.11	6.85	3.20	2.86	3.68
2.5	6.12	6.85	3.20	2.86	3.68
3.0	6.12	6.86	3.20	2.86	3.69
4.0	6.13	6.87	3.20	2.87	3.70
5.0	6.14	6.88	3.21	2.88	3.71
7.5	6.18	6.91	3.22	2.91	3.74
10.0	6.22	6.95	3.23	2.94	3.79
13.8	6.29	7.02	3.26	3.00	3.87

Table A.2: Efficiency of the Slab Phantom without a Slab behind the Source

Slab Thickness (cm)	Absolute Efficiency (%)				
	Cs-137	Co-60	Am-241	Ir-192	I-131
0.0	0.091	0.054	0.444	0.206	0.169
0.5	0.088	0.053	0.439	0.201	0.163
1.0	0.085	0.051	0.432	0.195	0.156
1.5	0.082	0.050	0.424	0.188	0.149
2.0	0.078	0.048	0.411	0.182	0.142
2.5	0.075	0.047	0.401	0.175	0.135
3.0	0.072	0.045	0.388	0.168	0.130
4.0	0.066	0.043	0.362	0.155	0.118
5.0	0.060	0.040	0.335	0.144	0.107
7.5	0.048	0.034	0.270	0.119	0.085
10.0	0.040	0.029	0.210	0.097	0.066
13.8	0.028	0.023	0.145	0.072	0.046

Table A.3: MDA for the Slab Phantom without a Slab behind the Source

Time (minutes)	Slab Thickness (cm)	MDA (nCi)				
		Cs-137	Co-60	Am-241	Ir-192	I-131
1	0.0	46.9	30.3	42.2	24.2	43.7
	0.5	48.2	30.8	42.6	24.8	45.3
	1.0	50.2	31.8	43.3	25.6	47.3
	1.5	52.2	32.8	44.1	26.5	49.4
	2.0	54.4	33.9	45.5	27.4	51.8
	2.5	56.9	35.0	46.6	28.5	54.4
	3.0	59.4	36.2	48.2	29.6	56.8
	4.0	64.7	38.2	51.7	32.2	62.4
	5.0	70.5	40.6	55.9	34.8	68.7
	7.5	87.9	47.9	69.4	42.0	86.7
	10.0	107.6	55.5	89.0	51.4	111.3
	13.8	149.8	72.4	129.5	69.8	159.6
5	0.0	20.6	13.3	18.7	10.7	19.3
	0.5	21.1	13.5	18.9	11.0	20.0
	1.0	22.0	13.9	19.2	11.4	20.9
	1.5	22.9	14.4	19.5	11.8	21.8
	2.0	23.8	14.8	20.1	12.2	22.9
	2.5	24.9	15.3	20.6	12.7	24.0
	3.0	26.0	15.8	21.3	13.2	25.1
	4.0	28.3	16.7	22.9	14.3	27.6
	5.0	30.9	17.7	24.7	15.4	30.4
	7.5	38.5	20.9	30.7	18.7	38.3
	10.0	47.1	24.2	39.4	22.8	49.1
	13.8	65.6	31.6	57.3	31.0	70.5
10	0.0	14.5	9.3	13.2	7.6	13.6
	0.5	14.8	9.5	13.3	7.8	14.1
	1.0	15.5	9.8	13.5	8.0	14.7
	1.5	16.1	10.1	13.7	8.3	15.4
	2.0	16.8	10.4	14.2	8.6	16.1
	2.5	17.5	10.8	14.5	8.9	16.9
	3.0	18.3	11.1	15.0	9.3	17.7
	4.0	19.9	11.7	16.1	10.1	19.4
	5.0	21.7	12.5	17.4	10.9	21.4
	7.5	27.1	14.7	21.6	13.2	27.0
	10.0	33.2	17.0	27.8	16.1	34.6
	13.8	46.2	22.2	40.4	21.9	49.7

APPENDIX B

ADDITIONAL LLNL PHANTOM DATA

Table B.1: MDA for the LLNL Realistic Torso Phantom

Time (minutes)	MDA (nCi)				
	Cs-137	Co-60	Ir-192	Am-241	I-131
1	55.5 ± 6.0%	34.4 ± 6.7%	27.3 ± 2.8%	47.2 ± 3.2%	51.8 ± 3.6%
5	24.3 ± 6.0%	15.0 ± 6.7%	12.1 ± 2.8%	20.9 ± 3.2%	22.9 ± 3.6%
10	17.1 ± 6.0%	10.6 ± 6.7%	8.6 ± 2.8%	14.7 ± 3.2%	16.1 ± 3.6%

Table B.2: MDI for the LLNL Phantom (nCi)

Days Post Intake	Cs-137	Co-60		Am-241	Ir-192			I-131
	F	M	S	M	F	M	S	F
0.25	64.7	32.5	31.8	45.2	32.5	26.3	25.7	62.5
0.50	83.4	39.9	38.9	55.6	41.9	32.4	31.6	82.2
0.75	106.8	48.3	47.0	67.3	53.8	39.3	38.3	107.6
1.00	136.7	58.2	56.0	81.0	69.1	47.4	45.7	140.7
1.25	176.2	68.7	65.8	95.7	89.2	56.2	53.8	185.3
1.50	226.4	80.2	76.2	111.6	114.9	65.7	62.4	243.2
1.75	290.7	92.1	86.8	128.1	147.9	75.6	71.3	319.1
2.00	373.2	103.8	97.2	144.5	190.3	85.5	80.0	418.6
2.25	478.8	115.8	107.6	161.1	244.7	95.5	88.8	548.8
2.50	614.9	127.0	117.3	176.7	315.0	105.0	97.0	720.1
2.75	791.4	137.6	126.1	191.4	406.4	114.0	104.5	946.9
3.00	1011.5	147.1	134.1	204.7	520.6	122.2	111.4	1236.6
4.00	2757.3	174.9	156.5	243.2	1432.5	146.6	131.2	3674.4
5.00	7498.5	190.0	167.7	264.1	3931.9	160.7	141.8	1.1E+04
6.00	2.0E+04	197.9	173.3	274.9	1.1E+04	168.8	147.9	3.2E+04
7.00	5.5E+04	202.9	176.5	281.8	3.0E+04	174.7	152.0	9.5E+04
Based on 10 Minute MDA (nCi)	17.1	10.6	10.6	14.7	8.6	8.6	8.6	16.1

Table B.3: MDD for the LLNL Phantom with a 10 Minute MDA (CEDE) (ICRP 26)

Days Post	Cs-137	Co-60		Am-241	Ir-192			I-131
Intake	F	M	S	M	F	M	S	F
0.25	2.07	1.07	6.95	2.01E+04	0.61	0.47	0.73	2.05
0.50	2.66	1.32	8.51	2.47E+04	0.79	0.59	0.89	2.70
0.75	3.41	1.60	10.29	2.99E+04	1.02	0.71	1.08	3.54
1.00	4.37	1.92	12.25	3.59E+04	1.30	0.86	1.29	4.63
1.25	5.63	2.27	14.38	4.25E+04	1.68	1.01	1.51	6.09
1.50	7.23	2.65	16.7	4.96E+04	2.17	1.19	1.76	8.00
1.75	9.28	3.05	19.0	5.69E+04	2.79	1.37	2.01	10.50
2.00	11.92	3.43	21.2	6.41E+04	3.59	1.54	2.25	13.77
2.25	15.3	3.83	23.5	7.15E+04	4.62	1.72	2.50	18.1
2.50	19.6	4.20	25.6	7.85E+04	5.94	1.90	2.73	23.7
2.75	25.3	4.55	27.6	8.50E+04	7.67	2.06	2.94	31.1
3.00	32.3	4.87	29.3	9.09E+04	9.82	2.21	3.14	40.7
4.00	88.0	5.78	34.2	1.08E+05	27.0	2.65	3.69	120.9
5.00	239	6.28	36.7	1.17E+05	74.2	2.90	3.99	358
6.00	651	6.54	37.9	1.22E+05	204	3.05	4.16	1061
7.00	1767	6.71	38.6	1.25E+05	558	3.15	4.28	3141

Table B.4: MDD for the LLNL Phantom with a 10 Minute MDA (CED) (ICRP 60)

Days Post	Cs-137	Co-60		Am-241	Ir-192			I-131
Intake	F	M	S	M	F	M	S	F
0.25	1.10	1.20	3.65	7.05E+03	0.22	0.51	0.63	1.71
0.50	1.42	1.48	4.48	8.67E+03	0.28	0.63	0.77	2.25
0.75	1.82	1.79	5.41	1.05E+04	0.36	0.76	0.93	2.95
1.00	2.32	2.15	6.44	1.26E+04	0.46	0.92	1.11	3.86
1.25	3.00	2.54	7.56	1.49E+04	0.60	1.08	1.31	5.08
1.50	3.85	2.97	8.76	1.74E+04	0.77	1.27	1.52	6.66
1.75	4.94	3.41	9.98	2.00E+04	0.99	1.46	1.74	8.74
2.00	6.34	3.84	11.17	2.25E+04	1.27	1.65	1.95	11.47
2.25	8.14	4.28	12.38	2.51E+04	1.63	1.84	2.17	15.0
2.50	10.45	4.70	13.49	2.76E+04	2.10	2.03	2.37	19.7
2.75	13.45	5.09	14.50	2.99E+04	2.71	2.20	2.55	25.9
3.00	17.2	5.44	15.4	3.19E+04	3.47	2.36	2.72	33.9
4.00	46.9	6.47	18.0	3.79E+04	9.55	2.83	3.20	100.7
5.00	127.5	7.03	19.3	4.12E+04	26.2	3.10	3.46	298
6.00	346	7.32	19.9	4.29E+04	71.9	3.26	3.61	884
7.00	941	7.51	20.3	4.40E+04	197	3.37	3.71	2616

APPENDIX C

PHANTOM SPECTRAL DATA

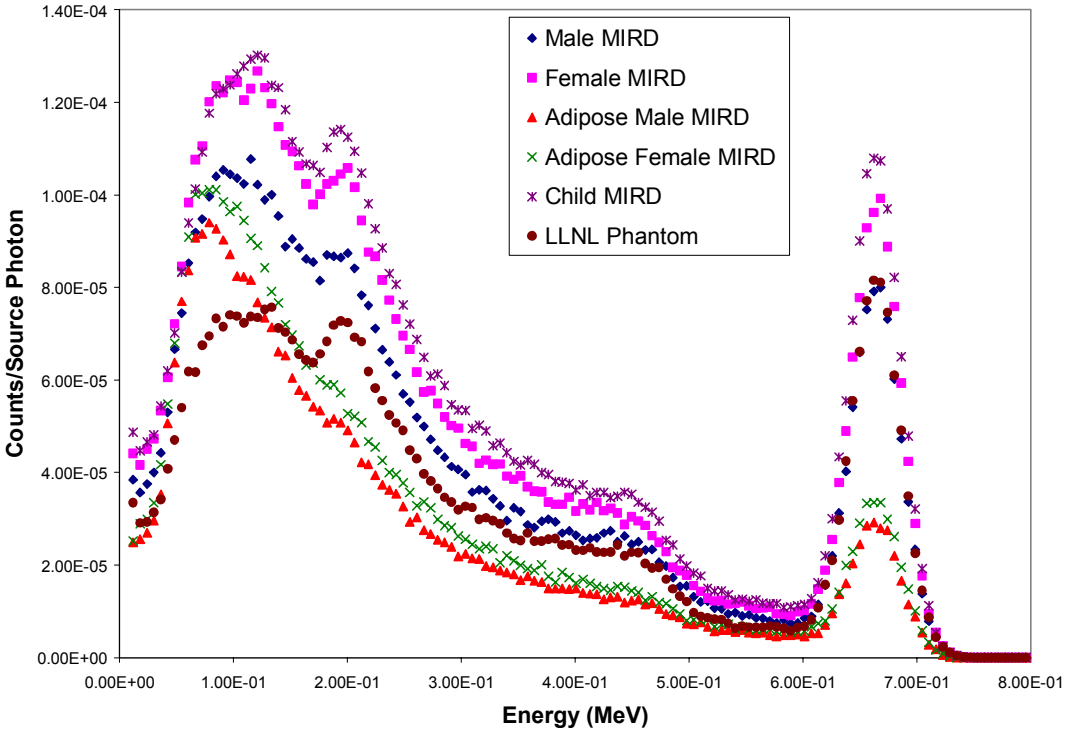

Figure C.1: MCNP Simulated ^{137}Cs Spectral Data

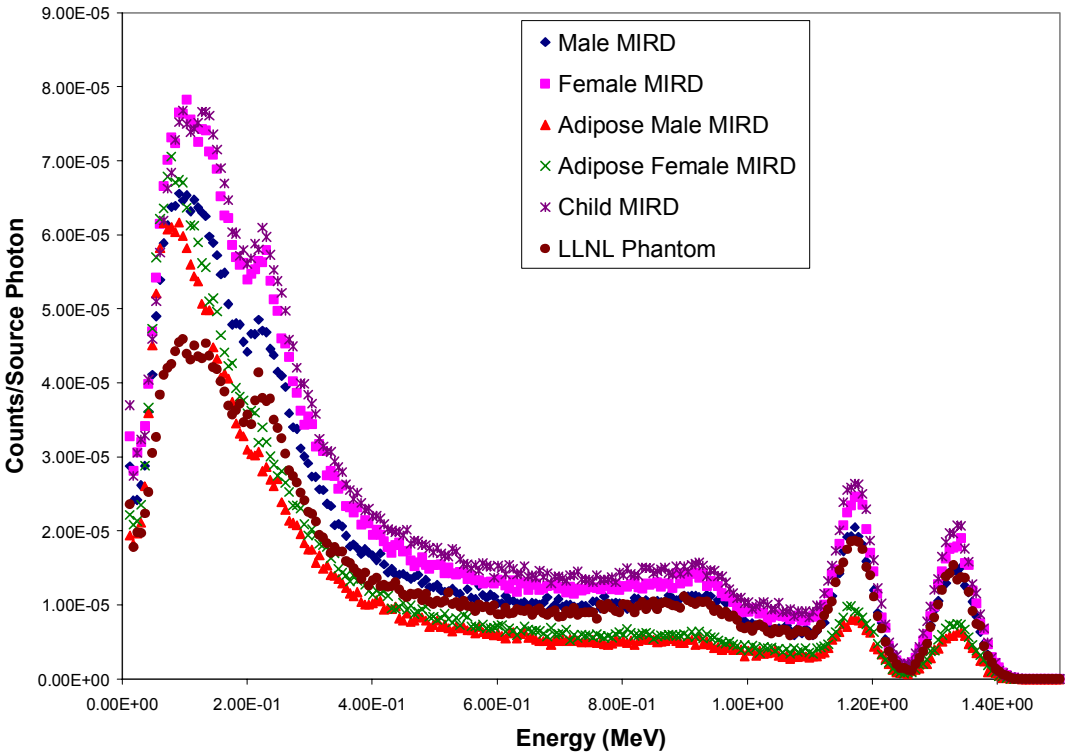

Figure C.2: MCNP Simulated ^{60}Co Spectral Data

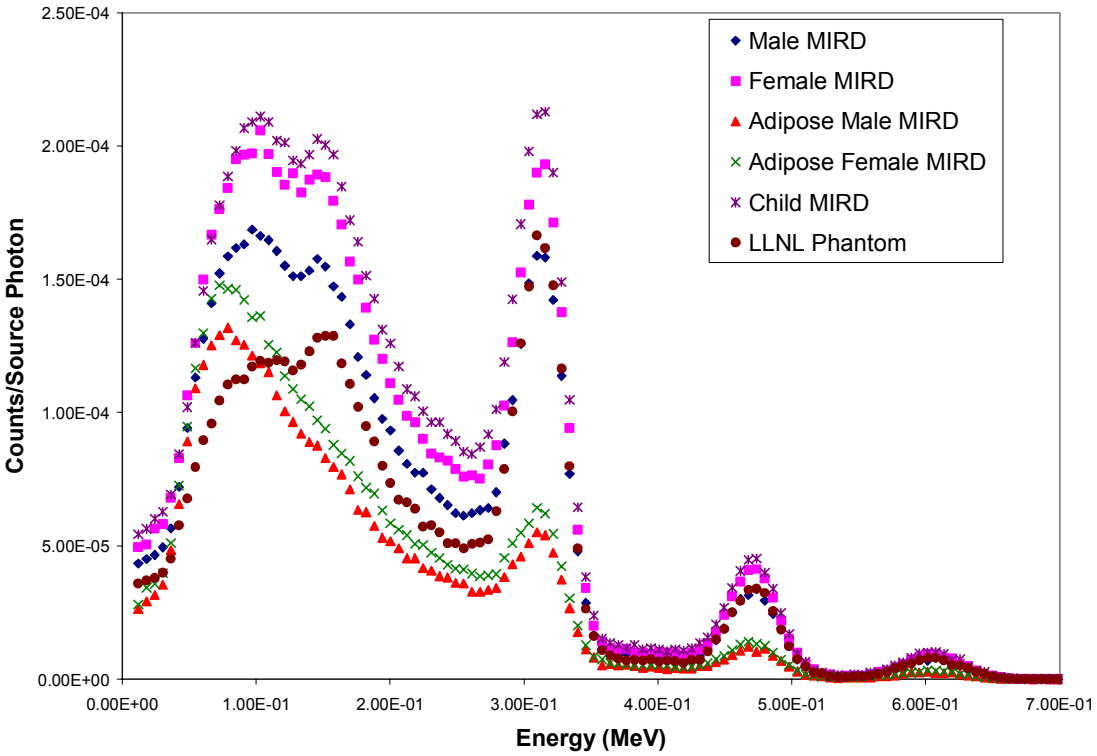

Figure C.3: MCNP Simulated ^{192}Ir Spectral Data

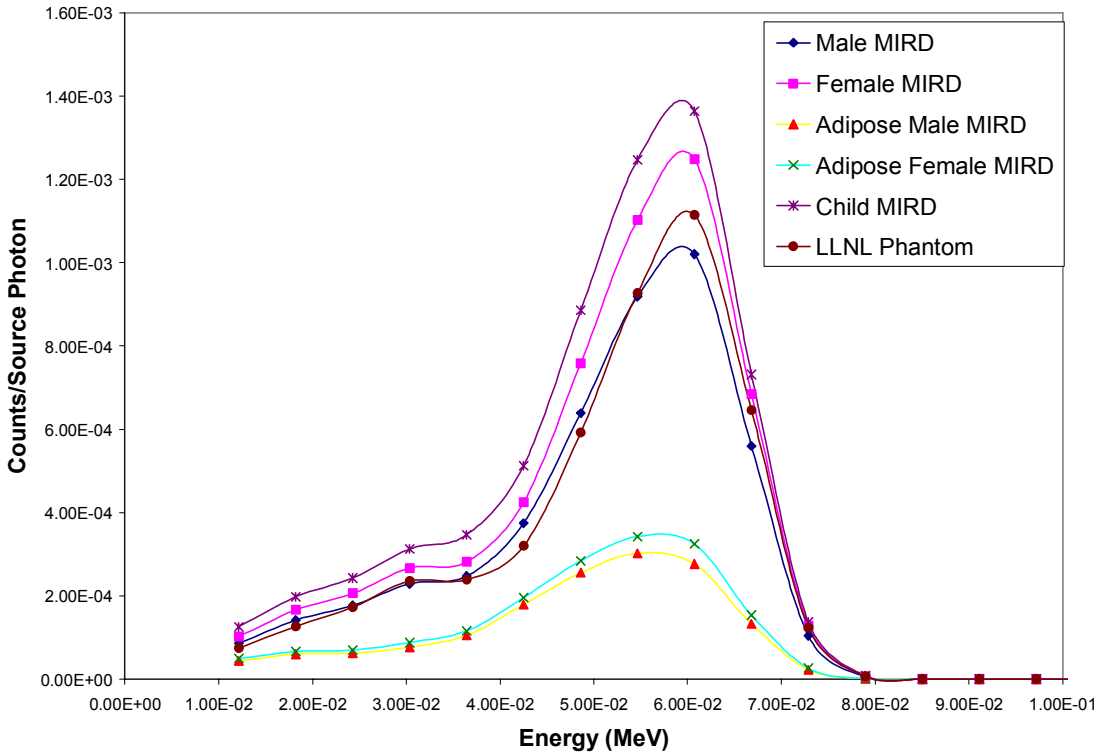

Figure C.4: MCNP Simulated ^{241}Am Spectral Data

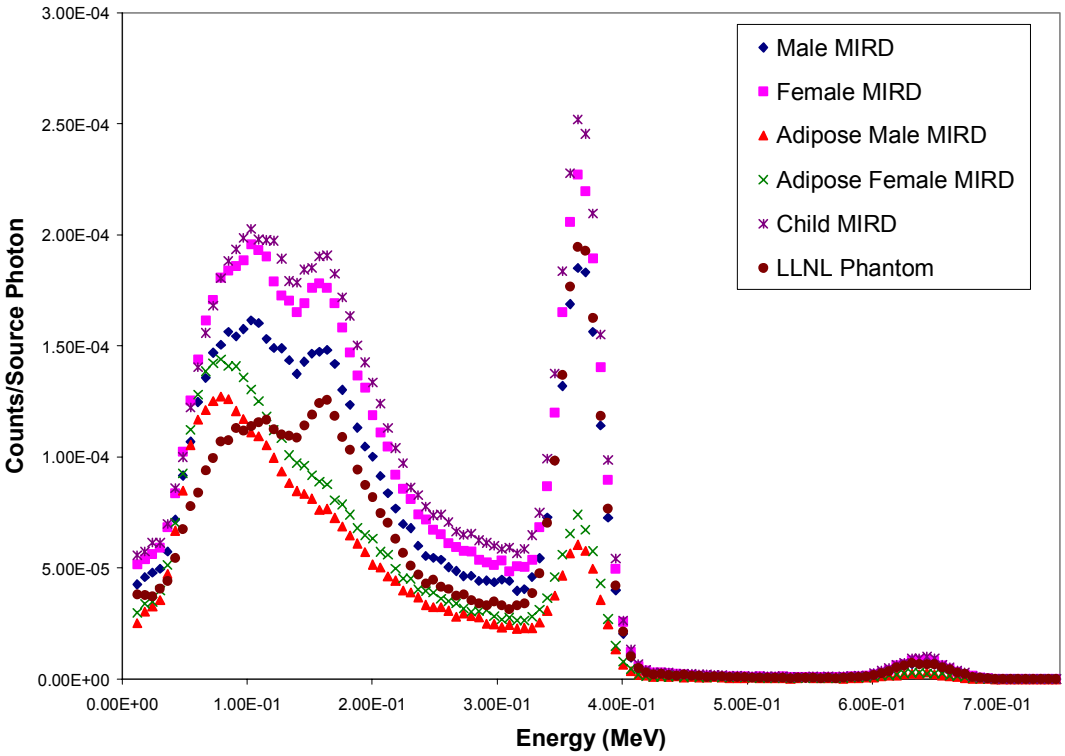

Figure C.5: MCNP Simulated ^{131}I Spectral Data

APPENDIX D

SLAB PHANTOM MCNP INPUT FILE

```
Slab Phantom with a 2.5 cm Slab Loaded
C Cell Cards
c   Exploranium GR-130
C   Detector Crystal
500 7 -3.667   -15 16 -17
C   Detector Housing
501 8 -.94   4 -5 6 -8
502 8 -.94   7 -5 -6
503 8 -.94   15 -3 5
504 8 -.94   4 -7 -6
505 8 -.94   -15 -16 5
C   Aluminum Plate
506 9 -1   10 -4 -8
C   Foam-like Material
507 10 -.92   -2 3
508 10 -.92   -3 8 -5
C   Casing
509 9 -1   -1 9 -11
C   Air Between casing & foam
510 1 -1.293e-3   -9 2
C   Rubber top
511 11 -1.34   -1 9 11
C   Plexiglas case
512 2 -1.19   12 -13
C   Plexiglas or air inside case
513 1 -1.293e-3   -12 -14
514 2 -1.19 -12 14
C   Air outside case
515 1 -1.293e-3   1 13 18 -99
c   Back Plexiglas
516 2 -1.19   -18
C   Outside Universe
999 0     99

C Surface Cards
C   Outer Casing
1   rpp -5.5 5.5 0 10 0 23.5
C   Foam-like Covering
2   rpp -3 3 2 8 4.5 23.3
3   rpp -2.4 2.4 2.6 7.4 4.9 23.29
C   Aluminum Plate
4   pz 5
c   Detector housing
5   pz 14.5
6   c/z 0 5 1.9
7   pz 10.7
```

```
8   c/z 0 5 2.3
9   rpp -5.3 5.3 .2 9 .2 23.3
10  pz 4.9
11  py 9
C   Plexiglas Case
12  rpp -14.9 14.9  -9.9 20.5 24.1 37.9
13  rpp -15.5 15.5 -10.5 20.5 23.5 38.5
c   This plane determines the thickness of the slab
c   For this input, the slab is 2.5 cm thick
c   37.9-35.4=2.5
14  pz 35.4
c   Detector Crystal
15  c/z 0 5.16 1.9
16  pz 17.59
17  pz 23.29
c   Back Plexiglas
18  rpp -15.5 15.5 -10.5 20.5 38.7 53.7
99  rpp -100 100 -100 100 -100 100

C Material Cards
c Material 1: Air
m1 7000 -.7552 8000 -.2319 18000 -.0129
C Material 2: Plexiglas
m2 6000 .3333 8016 .1333 1001 .5334
c Material 7: NaI
m7 11000 .5 53000 .5
c Material 8: Low density glass
m8 14000 .3333 8000 .6667
c Material 9: Low Density Aluminum
m9 1000 .6667 6000 .3333
c Material 10: Foam-like material
m10 1000 .6667 6000 .3333
c Material 11: Rubber
m11 1000 .6 6000 .4
sdef pos=0 5 38.6 erg=d2
c si2 l 1.17 1.33 $Co-60
c sp2 0.9986 0.9998
c si2 l 0.6617 $Cs-137
c sp2 0.851
si2 l 0.0595 $Am-241
sp2 0.359
c si2 l .3645 .637 $I-131
c sp2 0.812 0.0727
c si2 l 0.316508 0.468071 0.308457 0.295958 0.604415 0.612466 &
c    0.588584 0.484578 0.374485 0.416471 0.489039 0.884542 &
c    0.283267 $Ir-192
```

```
c sp2 0.828112 0.478317 0.300025 0.286692 0.0823143 0.0530902 &
c    0.0451487 0.0318395 0.00721065 0.00664146 0.00442905 &
c    0.00292323 0.00262431
f8:p 500
ft8 geb -.0050254 .0700037 -.0784113
e0 0 253i 1.542642
imp:p 1 16r 0
mode: p
nps 1e7
print
```

APPENDIX E

LLNL PHANTOM MCNP INPUT FILE (CONDENSED)

```
DICOM Scan Converted by Scan2MCNP
c
c DICOM/Image Files from Directory:
c C:\Documents and Settings\Jesson\My Documents\dicom\1cm
c IM58
c IM62
c IM66
c IM70
c IM74
c IM2
c IM6
c IM10
c IM14
c IM18
c IM22
c IM26
c IM30
c IM34
c IM38
c IM42
c IM46
c IM50
c IM54
c
c ++++++++++++++++++++++++++++++++++++++++++++++++++++++++++++++++
c
c     Cells
c
c ++++++++++++++++++++++++++++++++++++++++++++++++++++++++++++++++
c
c Voxel Cells
c
   11     2 -1.040000    13  -14    70  -84   104 -105
   12     1 -1.293e-3    13  -14    84  -94   104 -105
   13     1 -1.293e-3    14  -15    51  -63   104 -105
   14     2 -1.040000    14  -15    63  -68   104 -105
   15     4 -1.110000    14  -15    68  -78   104 -105
   16     2 -1.040000    14  -15    78  -85   104 -105
   17     1 -1.293e-3    14  -15    85  -94   104 -105
   18     1 -1.293e-3    15  -16    51  -62   104 -105
   19     2 -1.040000    15  -16    62  -66   104 -105
   20     4 -1.110000    15  -16    66  -78   104 -105
…
c Cells 1-10 are the lungs, made of combined voxels
  1     12  -0.250000    19  -20    61  -62   106 -107
                       :20  -21    60  -62   106 -107
```

```
                  :21  -22    60  -61   106 -107
                  :22  -23    59  -61   106 -107
                  :23  -24    58  -61   106 -107
                  :24  -25    58  -61   106 -107
                  :25  -26    59  -60   106 -107
                  :26  -27    59  -61   106 -107
                  :27  -28    59  -60   106 -107
                  :28  -29    59  -60   106 -107
                  :28  -29    60  -61   106 -107
                  :29  -30    60  -61   106 -107
                  :30  -31    60  -61   106 -107
…
c   Detector Information is the Same as in the Slab Phantom
c Outside of Voxels and Detector
c
 9998  1 -1.293e-3   -999 979 980 988 (-10:41:-51:94:-104:123)
 9999  0   999

c +++++++++++++++++++++++++++++++++++++++++++++++++++++++++++++++++
c
c     Surfaces
c
c +++++++++++++++++++++++++++++++++++++++++++++++++++++++++++++++++
c
c py Planes
c
   10 py -15.283208
   11 py -14.306646
   12 py -13.330084
…
   39 py 13.037090
   40 py 14.013652
   41 py 14.990214
c
c px Planes
c
   51 px -21.922579
   52 px -20.946017
   53 px -19.969455
…
   92 px 18.116463
   93 px 19.093025
   94 px 20.069587
c
c pz Planes
c
```

```
  104 pz -21.675000
  105 pz -19.675000
  106 pz -17.675000
…
  121 pz 12.325000
  122 pz 14.325000
  123 pz 16.325000
c Detector interaction
984 px -13.26243
985 px -2.26243
986 pz -9.835
987 pz .165
c Detector
C     Outer Casing
988   rpp -13.26243 -2.26243 -36.830084 -13.330084 -9.835 0.165
…
c outside Universe
  999 so 75

c ++++++++++++++++++++++++++++++++++++++++++++++++++++++++++++++++
c
c     Materials
c
c ++++++++++++++++++++++++++++++++++++++++++++++++++++++++++++++++
c Material 1: Air
m1 7000 -.7552 8000 -.2319 18000 -.0129
…
c Material 13: Water
m13 1000 .5 8000 .5
sdef par=2 x=d1 y=d2 z=d3 cel=d4 erg=d5 eff=1e-6
si1 -15 15
sp1 0 1
si2 -12 12
sp2 0 1
si3 -18 12
sp3 0 1
si4 l 1 2 3 4 5 6 7 8 9 10
sp4 v
c si5 l 1.17 1.33 $Co-60
c sp5 0.9986 0.9998
c si5 l 0.6617 $Cs-137
c sp5 0.851
si5 l 0.0595 $Am-241
sp5 0.359
c si5 l .3645 .637 $I-131
c sp5 0.812 0.0727
```

```
c si5 l 0.316508 0.468071 0.308457 0.295958 0.604415 0.612466 &
c    0.588584 0.484578 0.374485 0.416471 0.489039 0.884542 &
c    0.283267 $Ir-192
c sp5 0.828112 0.478317 0.300025 0.286692 0.0823143 0.0530902 &
c    0.0451487 0.0318395 0.00721065 0.00664146 0.00442905 &
c    0.00292323 0.00262431
f8:p 9988
ft8 geb -.0050254 .0700037 -.0784113
e0 0 253i 1.542642
imp:p 1 2929r 0
mode: p
nps 5e7
print
```

APPENDIX F

MALE MIRD PHANTOM MCNP INPUT FILE (CONDENSED)

```
C Male Phantom at  21.0 Years
C Weight = 73.14 kg (161.24lbs) Height = 179.00 cm (70.47 inches)
c ++++++++++++++++++++++++++++++++++++++++++
c
c   File Prepared by Body Builder
c   CopyRight 1996-2004, White Rock Science
c
c   This input file is for the use of
c   BodyBuilder License holder only.
c   Distribution is Prohibited.
c
c ++++++++++++++++++++++++++++++++++++++++++
c
c ++++++++++++++++++++++++++++++++++++++++++++++++
c        CELLS
c ++++++++++++++++++++++++++++++++++++++++++++++++
c       LEG BONES
c       ARM BONES
c       PELVIS
c       SPINE
c       SKULL & FACE
c       RIBS
c       CLAVICLES
c       SCAPULAE
c       ADRENALS
c       BRAIN
c       GALL BLADDER
c       ESOPHAGUS
c       STOMACH
c       SMALL INTESTINE
c       ASCENDING COLON
c       TRANSVERSE COLON
c       DESCENDING COLON
c       SIGMOID COLON
c       HEART
c       KIDNEYS
c       LIVER
c       LUNGS
c       PANCREAS
c       SPLEEN
c       TESTICLES
c       THYMUS
c       THYROID
c       URINARY BLADDER
c       PENIS & SCROTUM
c       SKIN
```

```
c          Trunk Skin
c         Penis & Scrotum Skin
c        Legs Skin
c           HEAD
c           NECK
c         OUTER TRUNK---ARMS & SCAPULAE
c         UPPER TRUNK---ABOVE RIBS
c         UPPER RIB CAGE
c         LOWER RIB CAGE
c         HIGH CHEST ORGANS
c         CHEST---LIVER LEVEL
c         LOWER TRUNK
c        LEGS
c         SURROUNDING AIR
c           air           OUTSIDE of NECK
c
c  Detector setup same as Slab Phantom
700   0              600
           imp:p =0

c ++++++++++++++++++++++++++++++++++++++++++++++++++
c          SURFACES
c ++++++++++++++++++++++++++++++++++++++++++++++++++
...
c ++++++++++++++++++++++++++++++++++++++++++++++++++
c
c         TRANSFORMATIONS
c ++++++++++++++++++++++++++++++++++++++++++++++++++
...
c ++++++++++++++++++++++++++++++++++++++++++++++++++
c      MATERIALS
c      Compositions from ORNL Report TM-8381
c ++++++++++++++++++++++++++++++++++++++++++++++++++
...
C Source Definition
sdef erg=d1 x=d2 y=d3 z=d4 par=2 cel=330
c si1 l 1.17 1.33 $Co-60
c sp1 0.9986 0.9998
c si1 l 0.6617 $Cs-137
c sp1 0.851
si1 l 0.0595 $Am-241
sp1 0.359
C si1 l .3645 .637 $I-131
C sp1 0.812 0.0727
si2 -13.7 13.7
sp2 0 1
```

```
si3 -7.6 7.6
sp3 0 1
si4 43.4 67.6
sp4 0 1
f8:p 9988
ft8 geb -.0050254 .0700037 -.0784113
e0 0 253i 1.542642
mode p
print
nps 5e7
```

REFERENCES

Brodsky, A., Johnson, R., Goans, R. (2004). Public Protection from Nuclear, Chemical, and Biological Terrorism. Health Physics Society Summer School. (Medical Physics Publishing, Madison, WI).

Exploranium Radiation Detection Systems (2001). GR-130 – miniSPEC: Portable Gamma Ray Spectrometer User Manual.

Ferguson, C. (2003). Reducing the Threat of RDDs. IAEA Bulletin, Volume 45, No. 1.

International Commission on Radiological Protection (ICRP). (1975). Report of the Task Group on Reference Man. ICRP Publication 23.

International Commission on Radiological Protection (ICRP). (1977). Recommendations of the ICRP. ICRP Publication 26. Annals of the ICRP, Volume 3, No. 1-4.

International Commission on Radiological Protection (ICRP). (1991). Recommendations of the ICRP. ICRP Publication 60. Annals of the ICRP, Volume 21, No. 1-3.

International Commission on Radiological Protection (ICRP). (2003). Basic Anatomical and Physiological Data for Use in Radiological Protection. ICRP Publication 89. Annals of the ICRP, Volume 32, No. 3-4.

International Commission on Radiation Units and Measurements (ICRU). (1992). Phantoms and Computational Models in Therapy, Diagnosis, and Protection. ICRU Report 48. Bethesda, MD.

Kramer, G. (2004). The LLNL Phantom Redesigned: Sacrilege or Progress. Presented at the 11th International Congress of the International Radiation Protection Association, Madrid, Spain.

Kramer, G., Burns, L., Yiu, S. (1997). Lung Counting: Evaluation of Uncertainties in Lung Burden Estimation Arising From a Heterogeneous Lung Deposition Using Monte Carlo Code Simulations. Radiation Protection Dosimetry, Volume 74, No. 3.

Kramer, G., Hauck, B. (1999). Efficiency Maps of the LLNL and JAERI Realistic Torso Phantoms Using a 70 mm Diameter Germanium Detector and Implications for the Minimum Detectable Activity. Radiation Protection Dosimetry, Volume 82, No. 2.

Kramer, G., Inn, K. (1991). A Summary of the Proceedings of the Workshop on Standard Phantoms for in vivo Radioactivity Measurement. Health Physics, Volume 61, No. 6.

Kramer, G, et al. (1998). A Virtual Torso Phantom and its Comparison to the LLNL and JAERI Torso Phantoms. Presented at the Bioassay Analytical and Environmental Radiochemistry Conference, Albuquerque, NM.

Peterson, S., April, J., Goldberg, G. (2005). Hand-Held Exploranium GR-130 miniSPEC Instrument. http://www.bhi-erc.com/opportunities/technology/documents/FY99_Fact_Sheets_pdf/SpectralGamma.pdf (Accessed September 20, 2005).

Potter, C. (2002). Intake Retention Fractions Developed from Models Used in the Determination of Dose Coefficients Developed for ICP Publication 68-Particulate Inhalation. Health Physics, Volume 83, No. 5.

U.S. Environmental Protection Agency (EPA). (1988). Limiting Values of Radionuclide Intake and Air Concentration and Dose Conversion Factors for Inhalation, Submersion, and Ingestion. Federal Guidance Report No. 11, EPA-520/1-88-020, Washington, D.C.

White Rock Science. (2004). BodyBuilder, www.whiterockscience.com/wrs.html. (Accessed October 14, 2005).

White Rock Science. (2003). Scan2MCNP UserManual.

X-5 Monte Carlo Team. (2003). MCNP – A General Monte Carlo N-Particle Transport Code, Version 5. LA-UR-03-1987.